Hydrothermal Pb-Zn ore formation in the Central Rhodopian Dome, south Bulgaria : review and new time constraints from Ar-Ar geochronology

Autor(en): **Kaiser-Rohrmeier, Majka / Handler, Robert / Quadt, Albrecht V.**

Objekttyp: **Article**

Zeitschrift: **Schweizerische mineralogische und petrographische Mitteilungen = Bulletin suisse de minéralogie et pétrographie**

Band (Jahr): **84 (2004)**

Heft 1-2: **Geodynamics and Ore Deposit Evolution of the Alpine-Carpathian-Balkan-Dinaride Orogenic System**

PDF erstellt am: **24.09.2024**

Persistenter Link: https://doi.org/10.5169/seals-63738

Schweizerische Mineralogische und Petrographische Mitteilungen 84, 37–58, 2004

Hydrothermal Pb–Zn ore formation in the Central Rhodopian Dome, south Bulgaria: Review and new time constraints from Ar–Ar geochronology

Majka Kaiser-Rohrmeier[1], *Robert Handler*[2], *Albrecht v. Quadt*[1] and *Christoph Heinrich*[1]

Abstract

Large lead-zinc mineralised metasomatic replacement bodies and vein swarms are associated with the Central Rhodopian Dome, south Bulgaria, which is interpreted as an Oligocene extensional core complex. Four ore fields occur in the vicinity of a low-angle detachment fault system, which is crosscut by rhyolitic dykes and ore veins. $^{40}Ar/^{39}Ar$ dating of white mica from veins and altered wall rocks is used to date the hydrothermal evolution and to relate the mineralisation to metamorphic uplift and silicic magmatism in the region.

$^{40}Ar/^{39}Ar$ plateau ages in coarse-grained muscovite separated from Mn-skarns and vugs in gneisses vary between 36 and 35 Ma and are interpreted as late-metamorphic crystallisation or early cooling ages. The age of 35.25 ± 0.36 Ma of pre-ore muscovite from Davidkovo ore field is also interpreted as a cooling age following metamorphism and subsequent updoming of the footwall of the complex at around 36–35 Ma. Sericitic alteration in gneisses adjacent to the ore veins yields ages of 31.21 ± 0.38 Ma and 31.55 ± 0.46 Ma placing an upper bracket on ore formation in the Madan ore field. Ages of hydrothermal muscovite connected to sulphide precipitation cluster around 30 Ma, placing a lower bracket on the age of Pb–Zn mineralisation. Another hydrothermal sericite age ranges down to ~26 Ma but it probably indicates local resetting by persisting geothermal activity. Rhyolitic dykes crosscut by the ore veins may be about 1–2 Ma older than these according to published U–Pb data on single zircons and similar in age to the Borovitsa caldera east of the Laki ore field. The close correspondence of hydrothermal and magmatic ages near 30 Ma and the small time difference of only ~5 Ma to the amphibolite facies metamorphism in the footwall of the dome indicate that hydrothermal and magmatic activity are both related to rapid tectonic and erosional denudation during late-orogenic collapse.

Keywords: Hydrothermal Pb–Zn vein mineralisation, metamorphic core complex, $^{40}Ar/^{39}Ar$ dating, Madan, Rhodopes, Bulgaria.

Introduction

The European Alpine–Balkan–Carpathian–Dinaride province is part of the Mesozoic to post-Mesozoic Tethyan Eurasian metallogenic belt, which extends from the Mediterranean region along the Alps and southeastern Europe through the Caucasus and the Himalaya to Burma, where it links up with the circumpacific metallogenic belt (Jankovic, 1997). With its characteristic abundance of base and precious metals it is one of the most prominent and oldest mining districts of Europe and the Middle East and one of the key factors for the development of civilised societies in this region. Having always been in the focus of economic and scientific interest, the belt looks back to a long research history. In the past ten years, due to political changes, mineral exploration programs have been revitalised in southeastern Europe. The purpose of these projects is to evaluate existing mineral resources and to explore for new deposits. This exploration-based research added substantial data about the mineral deposits, but left open many fundamental questions regarding the origin of the ores. Earlier work by Pereira and Dixon (1971) and Jankovic (1977) recognised the general genetic link between geodynamics and mineralisations at convergent margins. Traditionally, subduction was regarded as the only essential factor for mineralisation at convergent margins (Sawkins, 1984; Sillitoe, 1991; Lips, 2002). Thus, Mitchell (1996) and Jankovic (1997) related the numerous ore deposits of the Carpatho–Balkan region to subduction and calc-alkaline magmatism. These general models agree with those of continued magmatism of an active margin due to long-term consumption of lithosphere, but they cannot explain the basic observations that (1) ore formation is episodic and does not show a simple correlation with the abundance

[1] Isotope Geology and Mineral Resources, Department of Earth Sciences, ETH Zürich, Sonneggstr. 5, CH-8092 Zürich, Switzerland. <majka.kaiser@erdw.ethz.ch>
[2] Institute of Geology and Paleontology, University of Salzburg, Hellbrunnerstr. 34, A-5020 Salzburg, Austria.

0036-7699/2004/0084/37

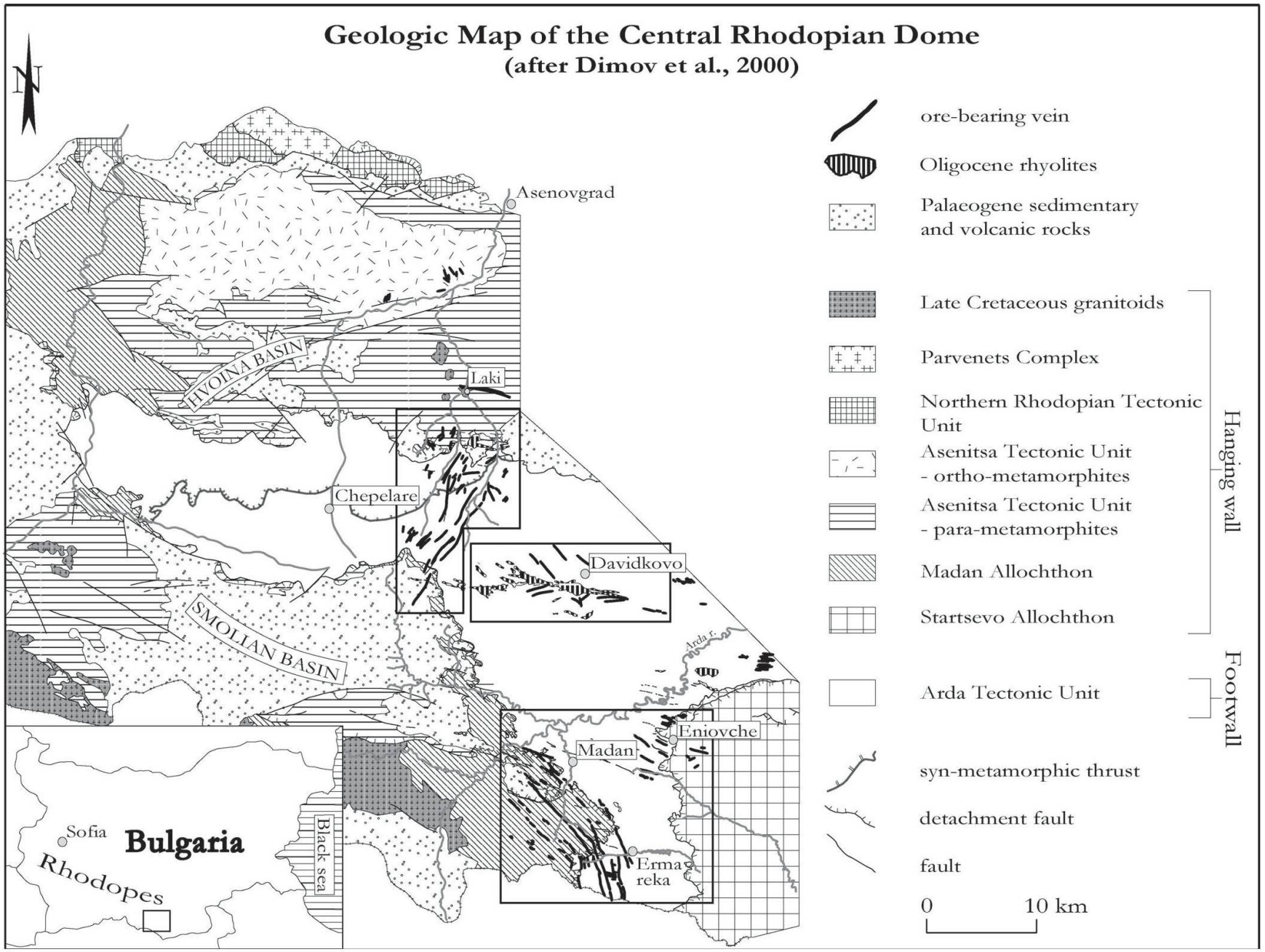

Fig. 1 Geological map of the Central Rhodopian Dome after Dimov et al. (2000).

of calcalkaline magmas (Silitoe, 1991; De Boorder et al., 1998) and that (2) some types of mineralisation in orogenic belts generally, and in the Alpine belt in particular, often occur in extensional settings late in the collisional history. Epithermal base- and precious-metal deposits in the Alpine–Balkan–Carpathian–Dinaride metallogenic belt, but also in Canada and the southwestern part of the USA are considered to be clearly associated with a Tertiary extensional regime (Spencer and Welty, 1986; Beaudoin et al., 1991; Beaudoin et al., 1992). Von Blanckenburg and Davies (1995) develop a slab breakoff model for syncollisional magmatism and tectonics in the Alps and based on new mantle-tomographic data, de Boorder et al. (1998) and Wortel and Spakman (2000) suggest that slab tear and slab detachment may be key elements in the geodynamic and metallogenic evolution of the Mediterranean–Carpathian region. They produce an increase in heat flow by emplacement of hot asthenosphere at shallow crustal levels, which may be responsible for the formation of hot mantle magmas, crustal melting and hydrothermal ore deposits. One aspect of our ongoing project in the framework of the GEODE program of the European Science Foundation (Blundell et al., 2002; Heinrich and Neubauer, 2002) aims at determining the critical mechanisms responsible for mineralisation in environments of late-orogenic collapse, following accretion of continental crust, high-grade metamorphism, extension and exhumation. In this paper, we report precise Ar–Ar geochronological data for geologically and paragenetically well-controlled samples defining the age of Pb–Zn mineralisation associated with the Central Rhodopian Dome of Bulgaria. These results lead to a first interpretation of the timing relationships between extension, metamorphic dome formation, silicic magmatism and hydrothermal ore formation.

Geological setting

Tectonic position of the Rhodope massif

The Rhodope massif extends in east–west direction in southern Bulgaria (Fig. 1) and northern Greece and comprises igneous and high-grade metamorphic rocks exposed over an area of about 300 km^2. It is situated at the southern border of the stable European continent and separated by the Maritsa suture from the Srednogorie and the Balkan mountains in northern and north-western direction. To the south-west, it is bordered by the Dinarides–Hellenides running parallel to the Adriatic coast. The Aegean sea, a Miocene to recent back-arc basin, limits the Rhodope massif in the southern and the eastern direction, where it disappears below the Neogene sedimentary cover of the Thracian basin (Ricou et al., 1998). In the past, the Rhodope massif had been interpreted as a Precambrian to Variscan continental fragment and described as a "Zwischengebirge" that remained unaffected by the Alpine evolution (Bonchev, 1915; Kober, 1928; Dimitrov, 1946), but the existence of Alpine magmatism and deformation has been demonstrated by Meyer (1968) and Meyer (1969) respectively. Remapping of the trust contacts during the last decades (Ivanov, 1988; Burg et al., 1990) revealed the existence of Alpine low-angle faults and synmetamorphic structures across the Rhodopian metamorphites. These observations caused a dramatic re-interpretation, and the Rhodope massif is now regarded as a complex of Mesozoic synmetamorphic nappes stacked in an Alpine active margin environment (Ricou et al., 1998). Its present structure is the product of Alpine compressional deformation culminating at about 110–90 Ma with large scale south-vergent thrusting, followed by emplacement of weakly deformed granitoid bodies at about 86–80 Ma (Peycheva et al., 1998). Final updoming and exhumation in the Tertiary occurred at about 40–35 Ma decreasing to 15 Ma at the eastern margin of the Strymon valley (Lips et al., 2000). Mposkos and Krohe (2000) report syncompressisonal extension in the eastern Rhodopes at about 42 and 32 Ma and postcollisional extension and core complex formation between 26 and 8 Ma, which is connected to magmatism. Extensional movement is clearly indicated as system of gently dipping detachment faults and syntectonic, asymmetric graben depressions which are filled with Paleogene (Eocene–Oligocene) continental clastics and locally abundant rhyolitic volcanics (Dimov et al., 2000).

Geology of the Central Rhodopian Dome

The Central Rhodopian Dome (Fig. 1) has been interpreted as a large (tens of km diameter) metamorphic core complex (Ivanov, 1989) in the central parts of the Rhodope massif. The pre-Paleogene basement consists mainly of high grade metamorphosed gneisses, mica-schists, amphibolites and marbles. A Cretaceous compressional phase has initiated amphibolite facies regional metamorphism of the basement and the formation of a system of synmetamorphic thrusts (Burg et al., 1990).

The contemporary structure of the Central Rhodopian Dome can be attributed to post-collisional crustal extension (Z. Ivanov in Dimov et

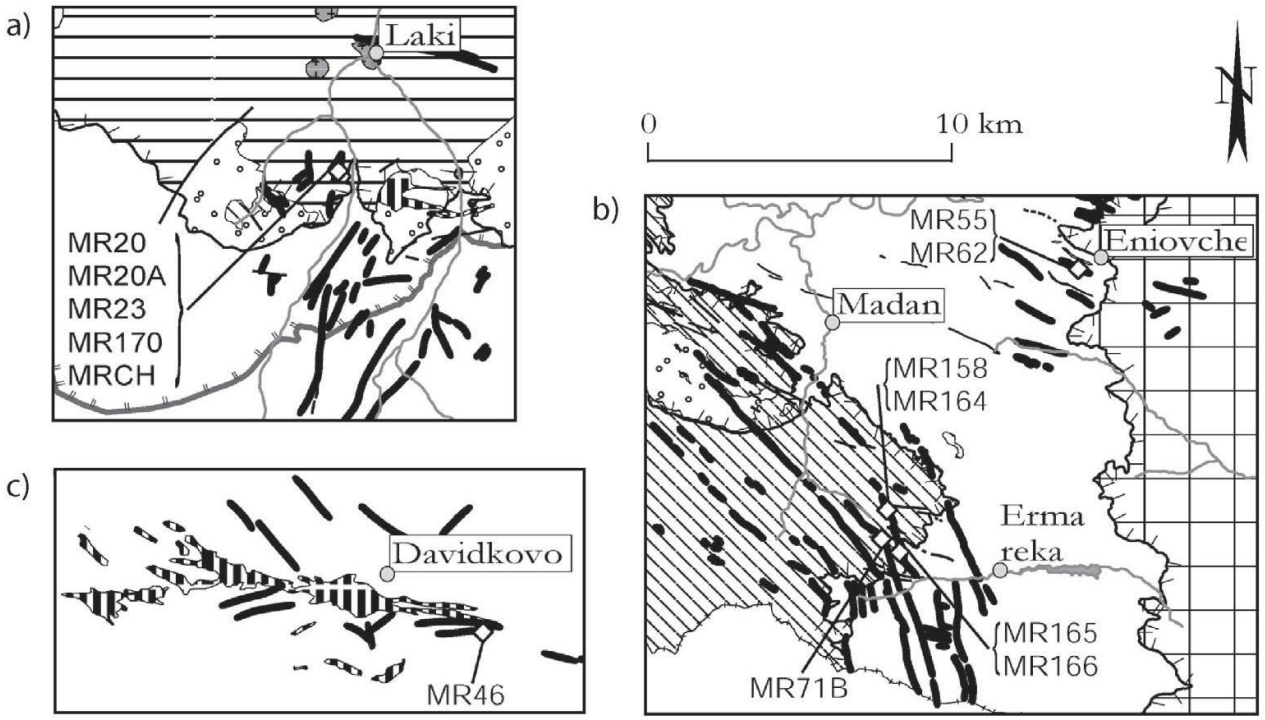

Fig. 2 Geology and sampling locations: (a) Laki ore field, (b) Madan ore field incl. Eniovche deposit, (c) Davidkovo ore field.

al., 2000), which generated a detachment fault system including a main flat-lying fault separating the Dome into a hanging wall and a footwall. It is a continuously mapped, outward-dipping fault zone characterised by a 3–20 m wide zone of brittle deformed and chloritised amphibole biotite gneiss; ductile deformation can be observed only in locally present calcite marble horizons. The footwall, known as Arda tectonic unit, consists of gneisses, micaschists, amphibolites and marbles. Migmatitisation and local anatexis are common and the locally latest leucosome gave U–Pb ages of about 37 Ma (Arkadaksky et al., 2000; Ovtcharova et al., 2003a). This age is interpreted to mark the peak of metamorphism (P = 4.5–6 kbar, T = 720–750 °C; Georgieva et al., 2002). The hanging wall of the northern part of the dome is predominantly represented by non-migmatised ortho-and parametamorphites of Asenitsa tectonic unit, but migmatised gneisses, amphibolites, mica-schists and marble packages of Madan allochthon also occur. The hanging wall of the southwestern part of the Dome consists both of rocks of Asenitsa tectonic unit and Madan allochthon. Above the hanging-wall, half-graben basins developed, which were filled with continental sediments of Eocene–Oligocene age (Dimov et al., 2000) and acidic sub-aereal volcanic rocks. The Startsevo allochthon, consisting of migmatised gneisses, amphibolites and marbles, overlies the detachment in the southeast.

The detachment is locally cut by rhyolitic dykes and shallow rhyolitic intrusives grading upward into volcanoclastic rocks. Rhyolitic lapilli tuffs also cover the central part of the dome at Davidkovo (Fig. 1), marking a paleo-landsurface at that time. Hydrothermal ore veins crosscut the detachment faults as well as some of the rhyolite dykes. Mineralisation is associated with carbonate-sericite alteration, which is particularly pervasive in overprinted rhyolitic dykes. These field relationships indicate that volcanism postdates not only extensional movement on the detachment, but also most of the uplift and denudation of the high-grade metamorphic rocks in the footwall of the core complex, whereas mineralisation postdates extensional movement of the detachment and occurred after uplift of the dome, and at least locally postdates acid magmatism.

Vein and replacement Pb–Zn deposits of the Central Rhodopian Dome

The Central Rhodopian Dome hosts several major Pb–Zn ore fields (Madan, Laki, and Davidkovo in Bulgaria and Thermes in Greece), all of which are spatially closely associated with the inferred detachment fault. The total amount of zinc and lead from at least 70 individual deposits and occurrences of the Central Rhodopian Dome is about 9 Mt out of which Madan ore field possess-

es 78% (Maneva et al., 1996). The richest and largest ore bodies were formed by hydrothermal replacement of marbles, but significant resources were mined from veins (Maneva et al., 1996). Presently three mines are active as underground operations (Laki-Djurkovo, Madan-Krushev Dol, and Eniovche) with an average production ore grade of 2.90% Pb and 2.16% Zn at Laki and 2.54% Pb and 2.10% Zn at Madan (Milev et al., 1996).

Structural control of ore emplacement

The deposits of the Central Rhodopian Dome comprise epi- to mesothermal Pb–Zn veins, disseminated vein stockworks and metasomatic replacements as the economically most important ore bodies. In all ore fields, the bulk of the economic ore is located within less than a kilometer above and below the detachment fault. Mineralised fractures sharply crosscut the detachment zone at Laki and Madan, where sulphide mineralisation locally extends up into conglomerates of the overlying extensional basins. The ore veins are hosted by uniform gneisses and several marble horizons and are predominantly controlled by intensive brittle deformation (Dimov et al., 2000; Dragiev and Danchev, 1990). The metasomatic ore bodies are formed by replacement where veins intersect marble horizons both in the foot wall and the hanging wall.

The *Laki ore field* (Fig. 1) is situated at the northern slope of the Central Rhodopian Dome and controlled by four linear ore-bearing NNE-trending fault zones. These faults cross the detachment and cut through thick-layered marbles in the upper part of the Asenitsa tectonic unit and through gneisses, schists, amphibolites and ultrabasites of the underlying Arda tectonic unit; sometimes the veins also crosscut subvolcanic rhyolitic dykes. The easternmost vein of Laki ore field is hosted in the terrigenous and volcanosedimentary units of the Borovitsa volcanic area. The ore bodies are mostly of vein type with lengths up to 7 km, but metasomatic ore bodies in marbles also occur with a spatial extension up to 140 m from the veins.

In the *Madan ore field* (Fig. 1), the deposits are closely related to NNW–SSE (320–340°) and WNW–ESE (280–320°) faults. The main vein mineralisation is developed along six subparallel NNW-trending faults with limited wallrock alteration (Bonev, 1982), whereas the WNW faults are not mineralised. Ore shoots are mainly situated in the NNW–SSE fault structures which offered a maximum of open space due to dextral strike-slip movement of the WNW-trending faults (Bonev, 1984). The barren WNW faults were essentially closed during ore deposition but subjected to deformation and alteration. The most extensively developed vein mineralisation is bound to the intersections between these two distinct types of faults (Dimov et al., 2000). The mineralisation can be traced to depths of 500–600 m below the surface; the veins show sharp contacts and reach a thickness up to 2 m, the network of stockwerk veinlets an extension of 10 m; they are often deformed by syn- and post-ore displacement (Bonev, 1982). Metasomatic replacement bodies are developed at the intersections of steep vein swarms with marble horizons which occur in the foot wall and the hanging wall. The thickness of the replacement ore bodies is controlled by the thickness of the marble horizons and reaches up to 5 m; lateral extension away from the feeding faults reaches 20–30 m but can extend up to 120 m at points of intersection of mineralised veins with the barren WNW faults. Minor ore deposits east of Madan include *Eniovche* (Fig. 1) and *Ardino* near the Startsevo detachment at the eastern contact of the Central Rhodopian Dome. In contrast to the other ore fields, the mineralisation at Eniovche is localised along WNW-trending fault structures which again cross the detachment. The ore bodies predominantly consist of 1.5–1.8 m thick veins, but metasomatic replacement ore bodies also occur in marbles of the hanging wall (Dimov et al., 2000).

In the central part of the dome, the *Davidkovo ore field* (Fig. 1), which was never mined on a larger scale, consists of 10 prospects and several occurrences. It is developed as stockworks and veins of up to 1 m thickness (Dimov et al., 2000) at the intersections of three NW-, E- and NE-trending fault structures in the foot wall of the dome. At Davidkovo, the detachment surface has been eroded completely and the mineralisation extends into subaereal lavas and volcanoclastic sediments (e.g. lavas or rhyolite domes and tuffs with accretionary lapilli) which were probably deposited onto an irregular land surface eroded into the lower unit of the dome. Sericitic alteration and minor veins overprint the volcanics, but significantly mineralised veins predominantly are hosted by gneisses and bodies of amphibolites.

Mineral paragenesis

In general, the ore fields of the Central Rhodopian Dome exhibit similar characteristics of mineralisation and a relatively uniform mineral association (Figs. 3a, b, c). The main minerals are quartz, galena, sphalerite, pyrite, arsenopyrite, chalcopyrite, calcite, rhodochrosite and other car-

bonates (Kolkovski et al., 1996; Bonev, 1982). Laki differs from the other ore fields by the absence of arsenic, which is common elsewhere, mostly as arsenopyrite. Minerals in veins and stockwerks are generally coarse, open-space infills with large crystals common in vugs, laterally grading into variably massive to porous sulphide ± carbonate ± quartz replacement orebodies zoned away from veins towards unaltered marble. Distal Mn-skarns dominated by johannsenite and rhodonite consistently occur at the outer contact of the replacement orebodies in contact with the original mar-

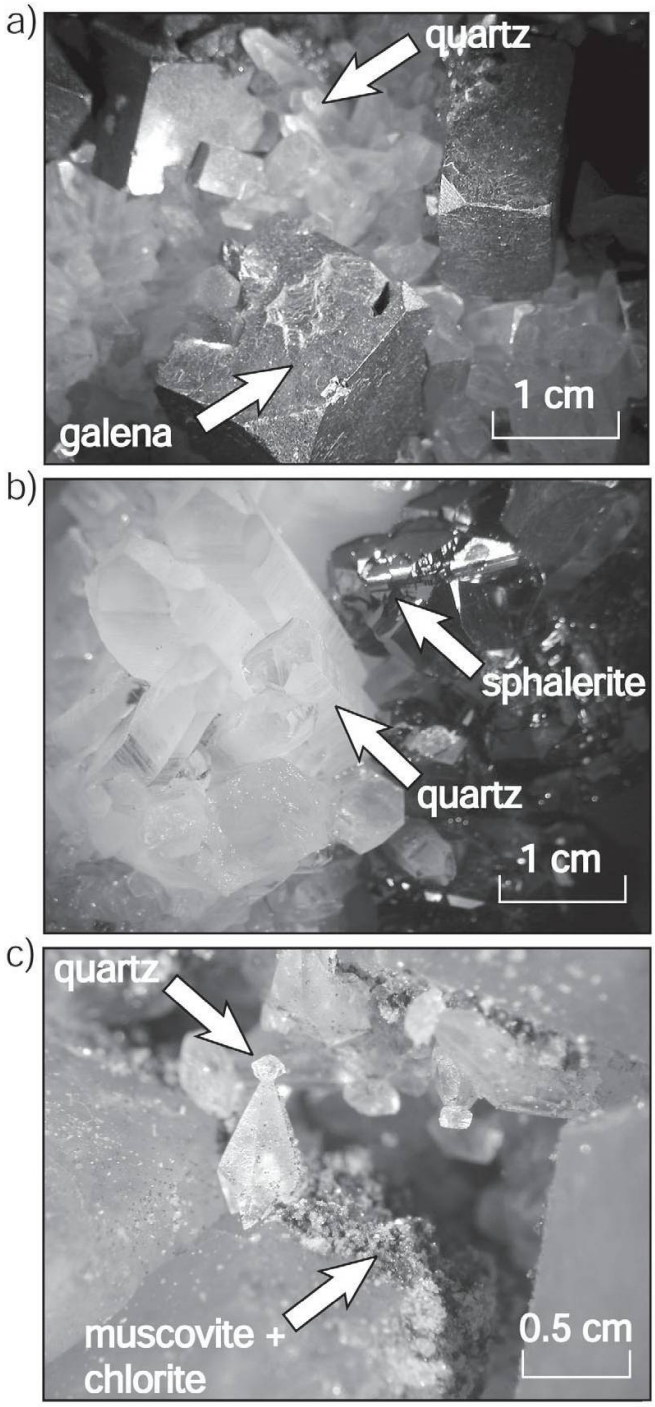

Fig. 3 Ore samples cristallised in open vugs of the Central Rhodopian Dome. (a) Galena and quartz, Madan ore field. (b) Sphalerite and quartz, Madan ore field. (c) Quartz with crustiform crystals of muscovite and chlorite, Laki ore field.

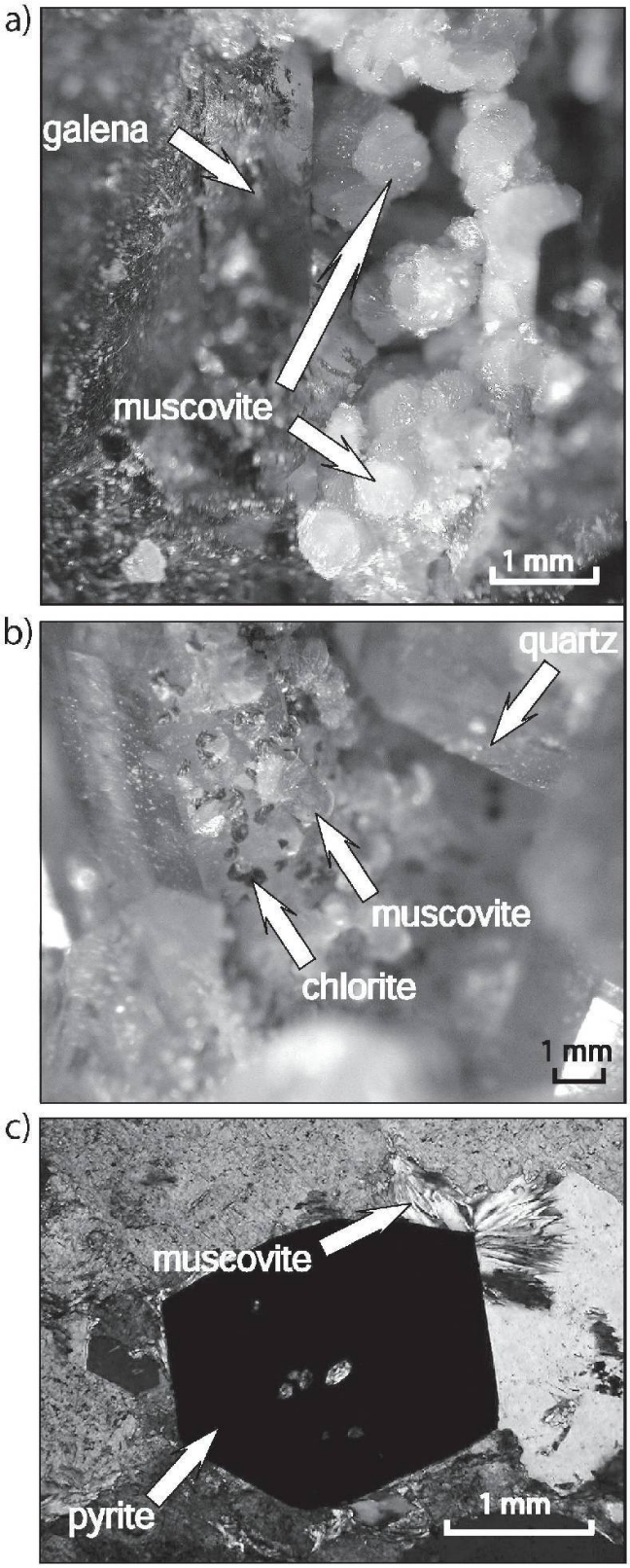

Fig. 4 White mica samples of the Central Rhodopian Dome. (a) Muscovite and galena, cristallised in open vug, Madan ore field. (b) Quartz, muscovite and chlorite, cristallised in open vug, Laki ore field. (c) Thin section with pyrite and muscovite from orebody of disseminated type, Eniovche deposit.

bles. Veins cutting gneisses show sericite alteration haloes of 0.1 to 2 m width, and regions with abundant stockwerk veinlets show a more extensive alteration of the surrounding gneisses

Table 1 Location, description and applied separation techniques of ore samples from three regions of the Central Rhodopian Dome.

	Sample Nr.	Locality	Sample description (separation techniques)
Laki ore field	MRCH	Djurkovo mine, l.762**	Crystallized in open vug: Quartz crystals in open vug overgrown by rosette-shaped and crustiform crystals of muscovite$^+$ and chlorite (scratching off, sieving >160 µm, handpicking)
	MR20	Djurkovo mine, l.762	Sericite$^+$ as open space filling in chloritized gneiss near front to Mn-skarn (washing, ultrasonic 5 min., sieving >315 µm, handpicking)
	MR20A	Djurkovo mine, l.762	Front to Mn-skarn in phlogopite-bearing marble: Radially arranged epidote, chlorite and corse-grained muscovite$^+$ parallel to front (scratching off, sieving >190 µm, handpicking)
	MR23*	Djurkovo mine, l.762	Crystallized in open vug: Chalcopyrite, quartz, galena and sphalerite in open vug overgrown by rosette-shaped and crustiform crystals of muscovite$^+$, chlorite and calcite (scratching off, ultrasonic 5 min., sieving >58 µm, handpicking)
	MR170*	Djurkovo mine	Crystallzed in open vug: Little galena and sphalerite overgrown by dominant quartz and little pyrite; calcite and a crust of rosette-shaped crystals of muscovite$^+$ and chlorite overgrows galena, sphalerite, quartz and pyrite (scratching off, ultrasonic 5 min., sieving >58 µm, handpicking)
Madan ore field	MR71B	Krushev dol mine, l.550, bl.1	Single grains of coarse-grained muscovite$^+$ in a matrix of white clay as open space filling in altered gneiss (washing, sieving >315 µm, handpicking)
	MR158 la*	Petrovitsa mine, bl.6***	Crystallized in open vug: Thin layer of muscovite and chlorite at the base of the sample overgrown by idiomorphic galena crystals; rosette-shaped muscovite$^+$ crystallized on galena; flat-shaped, clear rhomboedric calcite covers muscovite (scratching off, ultrasonic 5 min., sieving >58 µm, handpicking)
	MR 164*	Petrovitsa mine	Crystallized in open vug: Little quartz and pyrite with an overgrowth of rosette-shaped crystals of muscovite$^+$ covered by dominating surficially dissolved idiomorphic galena crystals; little quartz and sphalerite crystallized in clusters on dissolved galena; crust of flat-shaped rhomboedric calcite crystallized on sphalerite and quartz (scratching off, ultrasonic 5 min., sieving >58 µm, handpicking)
	MR165*	S-Petrovitsa mine, bl.6	Crystallized in open vug: Quartz crystals and few pyrite covered by rosette-shaped and crustiform muscovite$^+$ and chlorite; crust of calcite crystals as last phase (scratching off, ultrasonic 5 min., sieving >58 µm, handpicking)
	MR166*	S-Petrovitsa mine, bl.6	Crystallized in open vug: Octaedric disssolved galena, fresh galena and sphalerite overgrown by quartz, occasionally by pyrite; rosette-shaped crystals of muscovite$^+$ and chlorite crystallized in interstices and as overgrowing crustiform crystals on galena and sphalerite; pinkish, cloudy aggregates of (mangano-) calcite; clear and flat-shaped rhomboedric crystals of calcite as last phase (scratching off, ultrasonic 5 min., sieving >58 µm. handpicking)
	MR167 l*	Petrovitsa mine	Crystallized in open vug: Crustiform crystals of muscovite$^+$ and chlorite overgrown by large galena crystals with dissolved, vuggy surfaces (vugs as remnants of fluid inclusions); fresh sphalerite and and little quartz crystallized on galena; little chalcopyrite overgrows galena and sphalerite; rosette-shaped aggregates of muscovite grown in interstices as last phase (scratching off, ultrasonic 5 min., sieving >58 µm, handpicking)
Eniovche dep.	MR55	Eniovche mine	Alteration halo in gneissic host rock containing epidote, muscovite$^+$ and pyrite cut by quartz-, galena- and sphalerite-bearing ore vein (sawing out halo, crushing, sieving <315 µm, washing, handpicking)
	MR62 la	Eniovche mine	Disseminated pyrite in quartz-muscovite$^+$ matrix cut by sphalerite-galena-chalcopyrite-pyrite-calcite-muscovite-bearing vein. White mica grows preferably on pyrite (scratching off, crushing, sieving >100 µm, washing, handpicking)
Davidkovo ore f.	MR46 la	4 km south of Davidkovo	Disseminated galena, sphalerite and pyrite in muscovite$^+$-and quartz-rich vuggy hostrock; former vugs filled with quartz, galena, sphalerite, pyrite and fine-grained sericite which is preferably crystallized on pyrite (crushing, sieving >100 µm, washing, magnet separation (I=0.9 A), handpicking)

*Muscovite confirmed by XRD-analysis , ** l.=level, *** bl.=block
$^+$Mica generation processed for dating

bles. Veins cutting gneisses show sericite alteration haloes of 0.1 to 2 m width, and regions with abundant stockwerk veinlets show a more extensive alteration of the surrounding gneisses

Madan ore field and Eniovche deposit

At the Madan ore field, the mineralogy has been studied most extensively (Bonev, 1968; Kolkovski

and Petrov, 1972; Bonev, 1977; Piperov et al., 1977; Bonev, 1982; Bonev, 1984; Kolkovski et al., 1996; Maneva et al., 1996; Vassileva and Bonev, 2001; Kostova et al., 2004). The main minerals comprise quartz, galena, sphalerite and johannsenite, which is abundant in metasomatic replacement ore bodies; there, pyrite, chalcopyrite, arsenopyrite, (Mn-) carbonates and rhodonite can be found as well.

The Mn-skarns, entirely developed in the replaced marble horizons, show Mn-rich pre-ore mineral assemblages, which are represented by radiate and spherulitic aggregates of clinopyroxenes ranging from johannsenite to manganoan hedenbergite being replaced by rhodonite. Fibrous manganoan amphibole replaces the clinopyroxenes but preserves their radial texture. Rhodochrosite and manganoan calcite are the predominant minerals representing the "post-skarn" alteration; ilvaite of high Mn-content is formed after manganoan hedenbergite at this stage, which is transitional to the subsequent sulphide deposition because of small sphalerite crystals included in ilvaite.

The sulphide ore minerals are developed in open veins and in the more vein-proximal parts of the marble replacement bodies. The paragenetic sequence in the sulphide-rich ore bodies is typically (see Kostova et al., 2004): (1) quartz-pyrite, (2) galena-chalcopyrite-quartz-sericite-chlorite, (3) quartz-sphalerite-galena, (4) quartz-arsenopyrite-sulfosalts (5) quartz-(Mn-) calcite. In the open vein spaces, euhedral crystals of galena (Fig. 3a), quartz, and dark to yellow sphalerite, pyrite, chalcopyrite and carbonate are precipitated, with occasional intercalations and overgrowths of chlorite and muscovite crystals that are clearly precipitated into open space. Muscovite and chlorite are observed to be crystallised as idiomorphic fan-shaped "mica-rosettes" (Figs. 3c, 4a, 4b), as isolated crystals or as crusts that generally overgrow stage (3) of the paragenesis and probably stage (4). Sphalerite (Fig. 3b) is texturally related to and often intergrown with galena; pyrite and chalcopyrite occur in single crystals.

Gneiss and amphibolite wallrocks show bleached light-green haloes with quartz–sericite–carbonate–pyrite (proximal; 1–100 cm) and chlorite–carbonate–epidote alteration (Tzvetanov, 1976). Syn-ore alteration related to the quartz–galena–sphalerite veins also includes local silicifi-

Table 2 Identification of ore parageneses; each ore sample is assigned to one of them.

	Sample Nr.	Pre-ore minerals	Ore-related alteration	Ore-stage: Vein- and cavity fillings: Early			Late
		Muscovite - epidote - chlorite		Quartz - galena - sphalerite - chalcopyrite	Quartz - pyrite	Quartz - chlorite - muscovite	Calcite
Laki ore field	MRCH					X	
	MR20	X					
	MR20A	X					
	MR23			X			
	MR170				X		
			Quartz - muscovite - pyrite (-epidote)	Quartz-pyrite – chlorite – muscovite	Quartz - galena - sphalerite – chlorite – muscovite	Quartz - pyrite - chalcopyrite – muscovite	Calcite - mangano-calcite
Madan ore field	MR71B		X				
	MR158 Ia				X		
	MR 164				X		
	MR165			X			
	MR166				X		
	MR167 I				X		
Eniovche dep.	MR55		X		X		
	MR62 Ia			X	X	X	X
		Vuggy quartz - muscovite		Quartz - galena - sphalerite - muscovite			
Davidkovo ore field	MR46 Ia	X		X			

cation of the gneisses (Bonev, 1968). Silicification and kaolinite alteration predominantly occur in the upper levels of the vein systems, often correlated with arsenopyrite and sulfosalts.

Homogenisation temperatures of fluid inclusions from skarns of about 400 °C are reported by Kolkovski et al. (1978). Kostova and Petrov (2003) report homogenisation temperatures of 274–326 °C from quartz from the Yuzhna Petrovitza deposit in the Madan ore field. Studies on quartz of the sulphide assemblages yielded 280–360 °C and 200–280 °C for the late quartz-carbonate deposition (Kolkovski and Petrov, 1972; Maneva et al., 1996). The higher temperatures in the sulphide-stage (300–365 °C) relate to the early quartz–pyrite assemblage and 260–350 °C are indicated for the galena–quartz and quartz–galena–sphalerite phases (Kolkovski et al., 1996). The Eniovche deposit is spatially separated from the Madan ore field but shares the same structural orientations (Fig. 2b). Small metasomatic orebodies can be observed, but polymetallic quartz–sulphide veins with carbonate and white mica are predominant. They are surrounded by zones of intense alteration of gneisses with abundant pyrite, quartz, fine-grained sericite and a little carbonate.

Laki ore field

The Laki deposits are predominantly of vein type, but orebodies of massive or disseminated character hosted by Mn-skarns also occur. In the Mn-skarns, chlorite and radially arranged epidote crystals can be observed near the skarn front against fresh marble. In the open veins, galena is the dominant sulphide mineral, exceeding sphalerite. Chlorite and muscovite occur as greenish crusts mostly crystallised on quartz (Fig. 3c). Calcite or, more rarely, manganocalcite crystallises as the last phase on quartz and galena. Homogenisation temperatures of fluid inclusions in vein quartz from the main mineralisation stage range from 370 °C to 250 °C; from metasomatic ore bodies (Govedarnika deposit) they are reported to be about 300–320 °C (Kolkovski et al., 1978; Krasteva and Stoynova, 1988).

Davidkovo ore field

The Davidkovo ore field exhibits 30 different primary minerals, among them the main paragenetic stages quartz–pyrite, quartz–galena–sphalerite, rhodochrosite–manganocalcite–calcite, quartz and heulandite–stilbite. Mineralisation occurs in veins and rarely as linear stockworks. Some massive orebodies exhibit a porous texture of partially disintegrated white mica and quartz as pre-ore minerals; disseminated quartz, galena, sphalerite, pyrite and fine-grained white mica represent the ore stage. Homogenisation temperatures of fluid inclusions in quartz are in the range of 345–200 °C (Naphtali and Malinov, 1988).

Ore formation

The formation of the vein and replacement deposits in the Central Rhodopian Dome is probably related to several large hydrothermal systems. Ore deposition occurred mostly at temperatures between 370 to 260 °C based on fluid inclusion evidence. As fluid inclusions in transparent minerals do not commonly show clear boiling assemblages, the pressure of ore formation is unknown and homogenisation temperatures might have to be pressure-corrected. However, using extracts of large fluid inclusions in galena, Bonev (1984) and Bonev et al. (2000) identified boiling as process in the Madan ore field, indicating that homogenisation temperatures are close to true temperatures. Temperatures from 250 to 325 °C correspond to boiling pressures of 40–120 bars corresponding to hydrostatic depths of 0.4 to 1.2 km, or a little deeper if the fluid contained some CO_2 (for which there is no clear evidence). Hydrostatic conditions are likely in the light of the widespread open vugs throughout the vein and replacement ores. However, the Mn-skarns show no open spaces preserved and they could have formed at higher fluid pressures. Vassileva and Bonev (2001) suggested that the formation of the skarns was completed first and then followed by selective replacement of Mn-skarns by the galena–sphalerite–quartz ± carbonate ore bodies, rather than both being a product of simultaneously advancing reaction fronts. The energy source for driving the cooling hydrothermal system is broadly related to the formation of the Central Rhodopian Dome, but deciphering the contributions from metamorphic, magmatic and surface-related processes presents one of the key questions, which we approach in our ongoing project by detailed geochronology.

Previous geochronological data for the ore deposits

Pb–Pb–model ages of galena samples from the Madan ore field yielded values between 58 and 35 Ma, possibly reflecting variable lead contributions from a slightly older basement source (Amov et al., 1985; Amov et al., 1993). K–Ar analyses on hydrothermal white mica from the Enio-

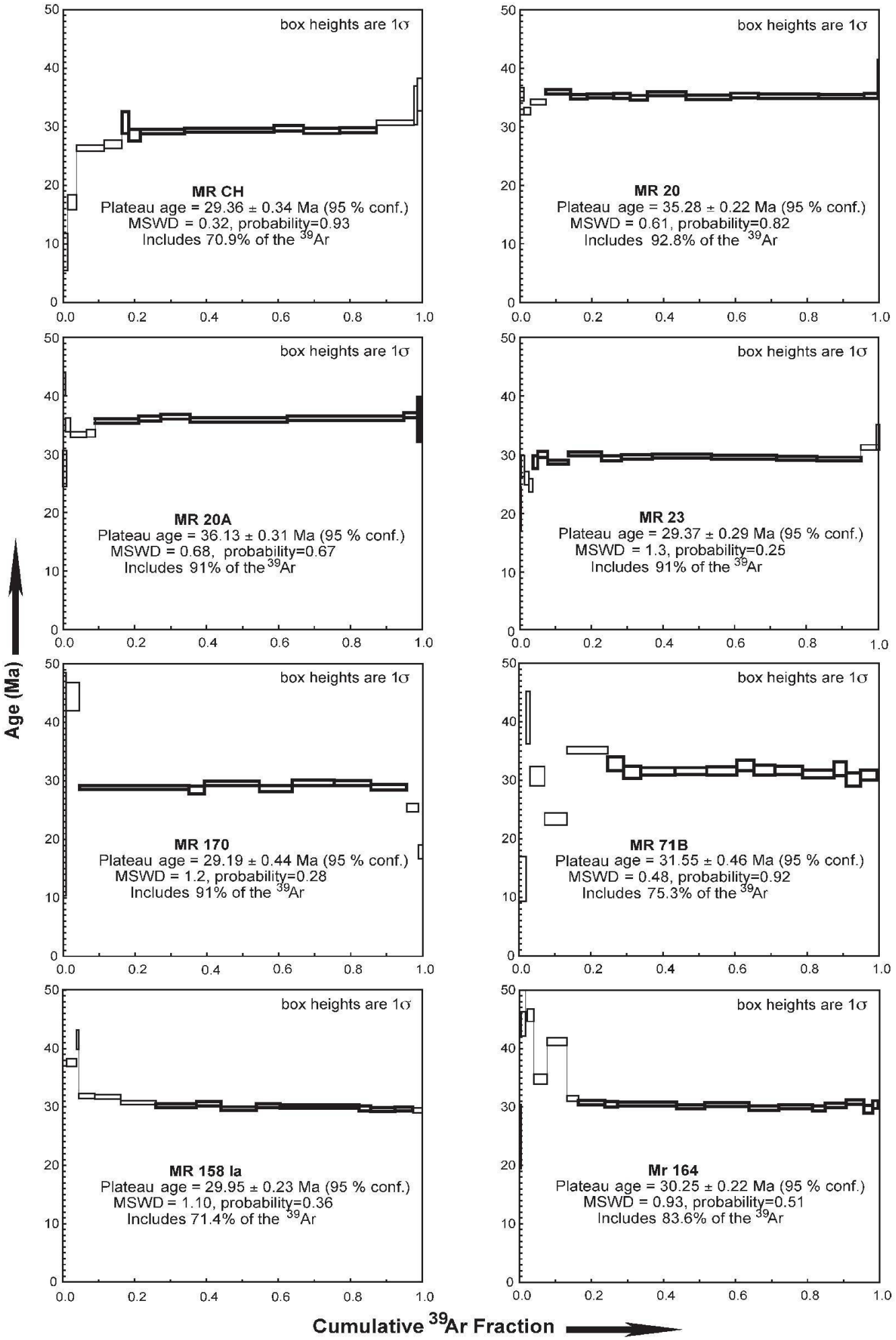
box heights are 1σ
MR CH
Plateau age = 29.36 ± 0.34 Ma (95 % conf.)
MSWD = 0.32, probability=0.93
Includes 70.9% of the 39Ar
box heights are 1σ
MR 20
Plateau age = 35.28 ± 0.22 Ma (95 % conf.)
MSWD = 0.61, probability=0.82
Includes 92.8% of the 39Ar
box heights are 1σ
MR 20A
Plateau age = 36.13 ± 0.31 Ma (95 % conf.)
MSWD = 0.68, probability=0.67
Includes 91% of the 39Ar
box heights are 1σ
MR 23
Plateau age = 29.37 ± 0.29 Ma (95 % conf.)
MSWD = 1.3, probability=0.25
Includes 91% of the 39Ar
box heights are 1σ
MR 170
Plateau age = 29.19 ± 0.44 Ma (95 % conf.)
MSWD = 1.2, probability=0.28
Includes 91% of the 39Ar
box heights are 1σ
MR 71B
Plateau age = 31.55 ± 0.46 Ma (95 % conf.)
MSWD = 0.48, probability=0.92
Includes 75.3% of the 39Ar
box heights are 1σ
MR 158 Ia
Plateau age = 29.95 ± 0.23 Ma (95 % conf.)
MSWD = 1.10, probability=0.36
Includes 71.4% of the 39Ar
box heights are 1σ
Mr 164
Plateau age = 30.25 ± 0.22 Ma (95 % conf.)
MSWD = 0.93, probability=0.51
Includes 83.6% of the 39Ar
Age (Ma)
Cumulative 39Ar Fraction

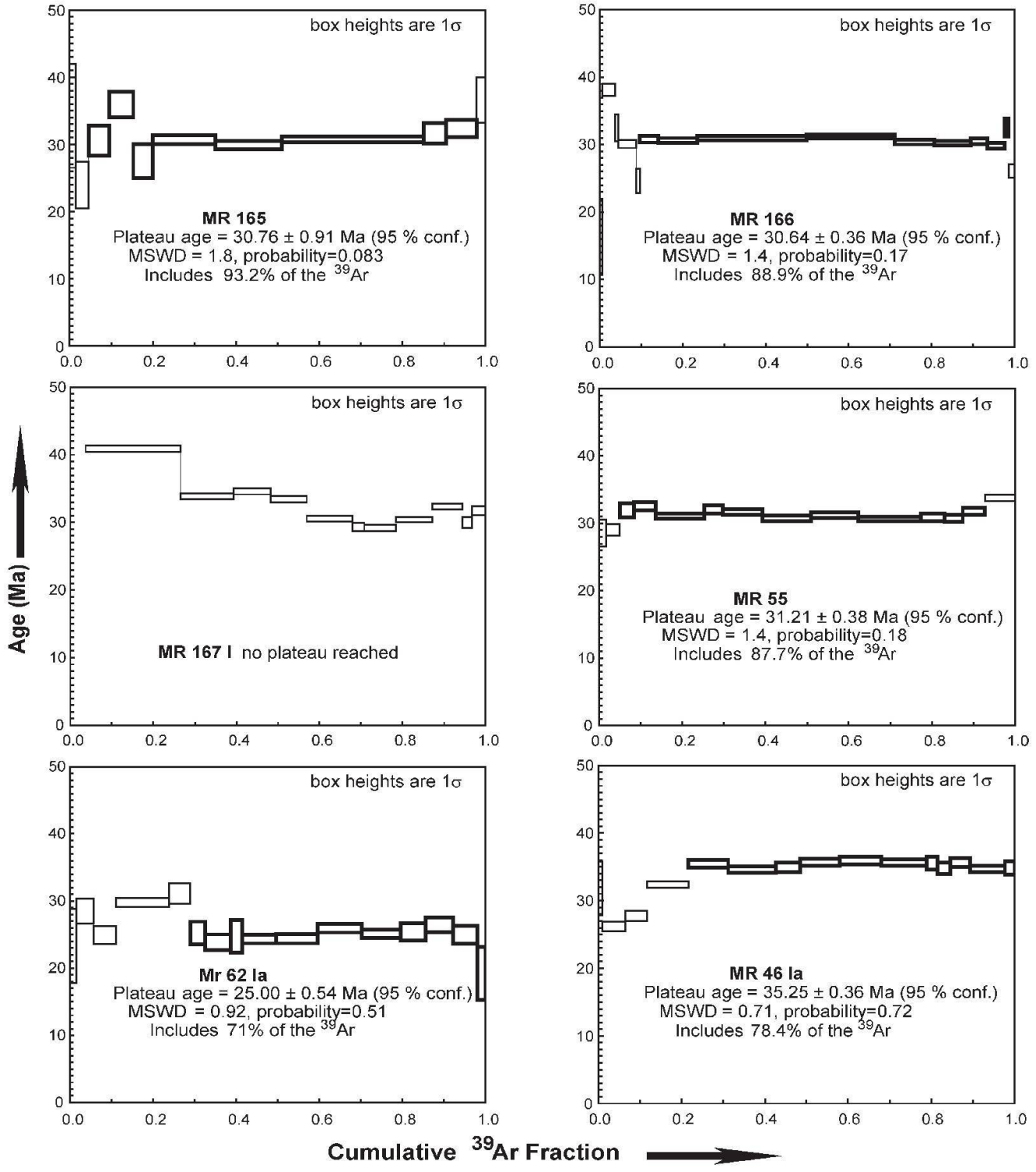

Fig. 5 $^{40}Ar/^{39}Ar$ age spectra with plateau ages of white micas from the Central Rhodopian Dome; bold boxes indicate steps maching the criteria for plateau ages after Ludwig (2001).

vche and Madan ore fields yielded ages of 33–31 Ma (P. Lilov reported in Dimov et al., 2000). In the Eastern Rhodopes, K–Ar studies of magmatic rocks of acid to more basic and alkaline compositions yielded ages between 37 and 25.5 Ma (Lilov et al., 1987). More recent studies (Singer and Marchev, 2000) of magmatism and hydrothermal activity of the Borovitsa caldera and the adjacent Spahievo ore district east of the Central Rhodopian Dome gave overlapping Ar–Ar data for acid magmatism and epithermal gold mineralisation between 32.2 and 32.1 Ma.

New Ar–Ar data of hydrothermal white micas

Sample selection

New samples from the four major ore fields of the Central Rhodopian Dome were obtained mainly

from underground exposures, where veins and metasomatic orebodies are unaffected by weathering (Fig. 2a–c, Table 1). White mica that can be unambiguously related to Pb–Zn mineralisation is widespread but rarely occurs in sufficient quantity and grain size for successsful separation and Ar–Ar dating. Where possible, two types of hydrothermal mica were collected from nearby locations, in an attempt to bracket the time of sulphide precipitation (Table 2). The first sample type contains sericite in the alteration halo of ore veins cutting gneissic rocks. This alteration can be so intense to leave a porous, mica-quartz dominated rock in which sulphides are subsequently precipitated, forming a disseminated ore type. These sericites could potentially predate, but at least the fine-grained sericite is probably synchronous with the beginning of hydrothermal fluid in-

Table 3 Analytical data of $^{40}Ar/^{39}Ar$ analyses of white micas from the Central Rhodopian Dome.

Step	$^{36}Ar/^{39}Ar$[a]	+/-	$^{37}Ar/^{39}Ar$[b]	+/-	$^{40}Ar/^{39}Ar$[a]	+/-	$\%^{40}Ar$[c]	$\%^{39}Ar$	age [Ma]	+/-
Sample:	**MR-CH**	J-Value: 0.01840 +/- 0.00018								
1	0.02259	0.00032	0.02408	0.00029	6.94792	0.09520	3.9	1.3	8.56	3.15
2	0.00752	0.00012	0.01550	0.00013	2.75524	0.03691	19.3	2.5	17.09	1.23
3	0.00269	0.00005	0.00692	0.00005	1.60675	0.01405	50.6	7.7	26.30	0.53
4	0.00178	0.00007	0.00482	0.00007	1.35928	0.01954	61.4	4.9	26.99	0.69
5	0.00021	0.00019	0.00307	0.00017	1.01028	0.05678	93.9	1.9	30.71	1.88
6	0.00027	0.00010	0.00188	0.00009	0.96186	0.02903	91.8	3.3	28.58	0.99
7	0.00001	0.00003	0.00154	0.00002	0.90309	0.00838	99.8	12.3	29.17	0.40
8	0.00005	0.00001	0.00144	0.00002	0.92277	0.00426	98.5	24.9	29.41	0.32
9	0.00004	0.00004	0.00114	0.00003	0.92945	0.01263	98.8	8.2	29.72	0.51
10	0.00006	0.00003	0.00126	0.00004	0.92093	0.00991	98.2	10.1	29.28	0.43
11	0.00008	0.00003	0.00121	0.00003	0.93049	0.00823	97.6	10.2	29.40	0.40
12	0.00018	0.00003	0.00379	0.00003	1.00013	0.00921	94.7	10.4	30.69	0.43
13	0.00001	0.00034	0.00402	0.00030	1.04307	0.10037	99.6	1.0	33.67	3.29
14	0.00028	0.00029	0.00372	0.00026	1.17705	0.08435	93.1	1.3	35.51	2.77
Steps 5 - 11								70.9	29.36*	0.34
Step	$^{36}Ar/^{39}Ar$	+/-	$^{37}Ar/^{39}Ar$	+/-	$^{40}Ar/^{39}Ar$	+/-	$\%^{40}Ar$	$\%^{39}Ar$	age [Ma]	+/-
Sample:	**MR-20**	J-Value: 0.02188 +/- 0.00022								
1	0.00864	0.00009	3.68275	0.00036	3.19172	0.02698	20.0	1.1	35.54	1.10
2	0.00287	0.00004	0.10190	0.00008	1.68942	0.01324	49.8	1.8	32.65	0.61
3	0.00237	0.00003	0.01338	0.00002	1.58847	0.00809	55.9	4.3	34.17	0.46
4	0.00067	0.00001	0.00916	0.00002	1.13213	0.00374	82.5	6.9	35.94	0.38
5	0.00029	0.00001	0.00634	0.00002	0.99965	0.00443	91.4	4.7	35.11	0.39
6	0.00040	0.00001	0.00608	0.00001	1.03395	0.00301	88.7	7.4	35.26	0.37
7	0.00027	0.00002	0.00513	0.00002	0.99678	0.00490	92.0	4.5	35.26	0.40
8	0.00022	0.00001	0.00471	0.00002	0.97495	0.00436	93.3	4.8	34.96	0.39
9	0.00019	0.00001	0.00501	0.00001	0.98279	0.00174	94.3	10.7	35.62	0.36
10	0.00014	0.00001	0.00352	0.00001	0.95281	0.00197	95.6	12.5	35.01	0.36
11	0.00008	0.00001	0.00233	0.00001	0.94411	0.00362	97.4	7.6	35.34	0.38
12	0.00008	0.00001	0.00180	0.00001	0.94026	0.00184	97.4	16.9	35.18	0.36
13	0.00009	0.00001	0.00167	0.00001	0.94249	0.00208	97.1	12.6	35.17	0.36
14	0.00016	0.00002	0.00263	0.00003	0.96334	0.00696	95.1	3.9	35.21	0.44
15	0.00019	0.00025	0.00118	0.00028	1.05423	0.07422	94.8	0.4	38.43	2.89
Steps 4 - 15								92.8	35.28	0.22
Step	$^{36}Ar/^{39}Ar$	+/-	$^{37}Ar/^{39}Ar$	+/-	$^{40}Ar/^{39}Ar$	+/-	$\%^{40}Ar$	$\%^{39}Ar$	age [Ma]	+/-
Sample:	**MR-20A**	J-Value: 0.02205 +/- 0.00022								
1	0.014697	0.000172	6.873738	0.000745	4.895618	0.050952	11.3	0.8	42.1	2.0
2	0.012290	0.000096	3.278107	0.000299	4.283180	0.028495	15.2	1.3	35.1	1.2
3	0.004599	0.000029	1.311596	0.000080	2.118713	0.008681	35.9	4.3	33.3	0.5
4	0.003216	0.000047	1.252062	0.000124	1.720469	0.013979	44.8	2.5	33.6	0.6
5	0.001416	0.000012	0.397978	0.000028	1.308691	0.003635	68.0	12.1	35.7	0.4
6	0.000809	0.000018	0.059507	0.000031	1.167068	0.005218	79.5	6.1	36.1	0.4
7	0.000541	0.000015	0.021808	0.000019	1.098493	0.004381	85.4	8.2	36.4	0.4
8	0.000145	0.000003	0.006411	0.000005	0.968668	0.001013	95.6	27.1	35.9	0.4
9	0.000120	0.000004	0.015904	0.000005	0.968114	0.001073	96.3	32.5	36.2	0.4
10	0.000100	0.000021	0.007038	0.000025	0.975744	0.006102	97.0	4.7	36.7	0.4
11	0.000542	0.000329	0.005652	0.000327	1.088605	0.097335	85.3	0.3	36.0	3.8
Steps 5 - 11								91.0	36.13	0.31

troduction. The second sample type consists of well-crystallised rosette-shaped or crustiform aggregates of muscovite, which could be confirmed by XRD analyses (Table 1). This type of muscovite overgrows quartz and sulphides in open vugs (Figs. 4a, 4b), but it can also be interlayered between multiple substages of sulphide deposition. More commonly it overgrows the main stage of galena, sphalerite and quartz deposition in open vugs and is only overgrown by the late calcite stage. This muscovite is at least partly synchronous or may immediately postdate hydrothermal

Table 3 (continued).

Step	$^{36}Ar/^{39}Ar$[a]	+/-	$^{37}Ar/^{39}Ar$[c]	+/-	$^{40}Ar/^{39}Ar$[a]	+/-	$\%^{40}Ar$[b]	$\%^{39}Ar$	age [Ma]	+/-
Sample:	**MR-23**	J-Value: 0.01849 +/- 0.00018								
1	0.00188	0.00038	0.01141	0.00045	1.19168	0.11171	53.3	0.4	20.60	3.69
2	0.00135	0.00018	0.00741	0.00020	1.25655	0.05410	68.2	0.9	27.88	1.80
3	0.00135	0.00011	0.00931	0.00015	1.19247	0.03328	66.6	1.2	25.82	1.12
4	0.00150	0.00011	0.00799	0.00017	1.19804	0.03370	63.1	1.1	24.56	1.14
5	0.00098	0.00011	0.00770	0.00011	1.16811	0.03214	75.2	1.3	28.58	1.09
6	0.00065	0.00005	0.01013	0.00007	1.11057	0.01346	82.8	2.8	29.92	0.53
7	0.00041	0.00003	0.00534	0.00003	1.00034	0.00751	87.8	5.7	28.56	0.38
8	0.00024	0.00001	0.00366	0.00002	0.99190	0.00394	92.9	9.2	29.98	0.32
9	0.00036	0.00003	0.00678	0.00004	1.00394	0.00832	89.5	5.5	29.23	0.40
10	0.00023	0.00002	0.00646	0.00003	0.97359	0.00517	93.0	8.6	29.45	0.34
11	0.00019	0.00001	0.00560	0.00002	0.96596	0.00270	94.2	16.4	29.59	0.31
12	0.00023	0.00001	0.00534	0.00002	0.97154	0.00267	93.1	18.1	29.42	0.30
13	0.00027	0.00001	0.00549	0.00002	0.97877	0.00418	91.7	11.1	29.20	0.32
14	0.00031	0.00001	0.00512	0.00002	0.98640	0.00318	90.8	12.2	29.13	0.31
15	0.00061	0.00003	0.00312	0.00004	1.13559	0.00929	84.2	4.8	31.10	0.43
16	0.00090	0.00022	0.00208	0.00021	1.27783	0.06425	79.1	0.7	32.91	2.13
Steps 5 - 14								91.0	29.37	0.29
Step	$^{36}Ar/^{39}Ar$	+/-	$^{37}Ar/^{39}Ar$	+/-	$^{40}Ar/^{39}Ar$	+/-	$\%^{40}Ar$	$\%^{39}Ar$	age [Ma]	+/-
Sample:	**MR-170**	J-Value: 0.01905 +/- 0.00019								
1	0.78824	0.00169	0.01136	0.00037	233.80366	0.56382	0.4	0.9	29.44	19.07
2	0.07225	0.00024	0.00967	0.00010	22.67383	0.07024	5.8	3.6	44.41	2.40
3	0.00207	0.00002	0.00953	0.00002	1.47122	0.00446	58.5	30.5	28.84	0.32
4	0.00136	0.00006	0.00510	0.00008	1.25167	0.01702	67.9	4.3	28.47	0.64
5	0.00226	0.00002	0.00488	0.00002	1.55021	0.00589	57.0	15.3	29.60	0.35
6	0.00196	0.00004	0.00478	0.00003	1.43528	0.01202	59.7	9.2	28.70	0.50
7	0.00234	0.00003	0.00406	0.00003	1.57674	0.00984	56.2	11.6	29.69	0.44
8	0.00219	0.00003	0.00426	0.00004	1.53230	0.00883	57.7	10.3	29.63	0.42
9	0.00214	0.00004	0.00403	0.00005	1.49550	0.01120	57.7	9.9	28.90	0.48
10	0.00201	0.00006	0.00430	0.00010	1.35463	0.01829	56.1	3.2	25.43	0.67
11	0.00248	0.00012	0.00675	0.00024	1.26935	0.03510	42.3	1.2	17.86	1.21
Steps 3 - 9								91.0	29.19	0.44
Step	$^{36}Ar/^{39}Ar$	+/-	$^{37}Ar/^{39}Ar$	+/-	$^{40}Ar/^{39}Ar$	+/-	$\%^{40}Ar$	$\%^{39}Ar$	age [Ma]	+/-
Sample:	**MR-71B**	J-Value: 0.02200 +/- 0.00022								
1	0.20353	0.00032	0.05356	0.00014	60.48655	0.09758	0.6	2.1	13.14	3.85
2	0.08150	0.00039	0.05410	0.00029	25.13217	0.11571	4.2	0.9	40.70	4.51
3	0.05825	0.00014	0.04697	0.00008	18.00464	0.04082	4.4	4.1	30.69	1.62
4	0.03828	0.00008	0.03840	0.00005	11.91625	0.02520	5.1	6.2	23.40	1.01
5	0.01471	0.00005	0.02448	0.00003	5.25480	0.01351	17.3	11.3	35.15	0.63
6	0.00779	0.00010	0.01901	0.00008	3.15032	0.02926	26.9	4.4	32.77	1.19
7	0.00461	0.00008	0.01758	0.00007	2.17369	0.02510	37.3	4.7	31.37	1.03
8	0.00703	0.00005	0.01508	0.00004	2.89233	0.01396	28.2	9.6	31.54	0.63
9	0.00657	0.00004	0.01579	0.00004	2.75929	0.01310	29.6	8.8	31.56	0.60
10	0.00609	0.00006	0.01554	0.00004	2.61573	0.01692	31.2	8.4	31.59	0.73
11	0.00453	0.00007	0.01361	0.00007	2.18138	0.02109	38.6	4.7	32.54	0.88
12	0.00456	0.00007	0.01531	0.00006	2.16812	0.01958	37.9	5.8	31.73	0.83
13	0.00492	0.00006	0.01265	0.00004	2.27541	0.01678	36.1	7.6	31.72	0.73
14	0.00481	0.00005	0.01227	0.00004	2.22629	0.01506	36.1	8.7	31.07	0.66
15	0.00377	0.00010	0.01229	0.00008	1.94216	0.02955	42.6	3.5	31.96	1.20
16	0.00385	0.00009	0.01041	0.00008	1.91731	0.02752	40.7	3.9	30.13	1.12
17	0.00428	0.00008	0.01135	0.00006	2.06273	0.02327	38.7	5.2	30.83	0.96
Steps 6 - 17								75.3	31.55	0.46

metal introduction. A third type of sample includes flaky muscovite, sometimes deformed and aligned along the original high-grade metamorphic fabric, taken in immediate contact with veins and alteration fronts in order to investigate the degree of hydrothermal resetting of metamorphic muscovites by the Pb–Zn-mineralising fluids.

Analytical techniques

The separation procedure used to obtain muscovite concentrates is listed in Table 1. Handpicked, 98% pure mineral concentrates are packed in aluminium-foil and loaded in quartz vials. For calculation of the J-values, flux-monitors are placed

Table 3 (continued).

Step	$^{36}Ar/^{39}Ar^a$	+/-	$^{37}Ar/^{39}Ar^b$	+/-	$^{40}Ar/^{39}Ar^a$	+/-	$\%^{40}Ar^c$	$\%^{39}Ar$	age [Ma]	+/-
Sample:	**MR-158 Ia**	J-Value: 0.01856 +/- 0.00019								
1	0.17977	0.00029	0.00398	0.00008	57.46205	0.08856	7.6	1.1	139.31	3.05
2	0.01294	0.00006	0.00359	0.00004	4.97332	0.01735	23.1	2.7	37.56	0.68
3	0.00754	0.00017	0.00473	0.00015	3.49776	0.04952	36.3	0.7	41.53	1.67
4	0.00202	0.00002	0.00609	0.00004	1.57241	0.00724	62.1	4.4	31.89	0.40
5	0.00164	0.00002	0.00448	0.00002	1.45492	0.00549	66.8	7.3	31.75	0.36
6	0.00123	0.00001	0.00305	0.00001	1.30391	0.00341	72.1	9.8	30.69	0.32
7	0.00120	0.00001	0.00279	0.00001	1.27976	0.00393	72.3	11.2	30.21	0.33
8	0.00112	0.00002	0.00242	0.00002	1.26675	0.00546	73.8	6.8	30.53	0.35
9	0.00034	0.00001	0.00230	0.00001	1.01071	0.00384	90.0	9.8	29.69	0.32
10	0.00038	0.00001	0.00198	0.00002	1.03610	0.00370	89.2	6.7	30.18	0.32
11	0.00045	0.00001	0.00191	0.00001	1.05468	0.00173	87.3	22.0	30.08	0.30
12	0.00022	0.00003	0.00183	0.00003	0.97422	0.00839	93.5	3.2	29.73	0.40
13	0.00025	0.00001	0.00197	0.00002	0.97817	0.00362	92.4	6.8	29.52	0.32
14	0.00023	0.00002	0.00175	0.00002	0.97611	0.00537	93.0	4.9	29.65	0.34
15	0.00025	0.00003	0.00199	0.00004	0.97551	0.00909	92.4	2.6	29.42	0.42
Steps 7 - 14								71.4	29.95	0.23
Step	$^{36}Ar/^{39}Ar$	+/-	$^{37}Ar/^{39}Ar$	+/-	$^{40}Ar/^{39}Ar$	+/-	$\%^{40}Ar$	$\%^{39}Ar$	age [Ma]	+/-
Sample:	**MR-164**	J-Value: 0.01865 +/- 0.00019								
1	0.22356	0.00053	0.00344	0.00017	66.82173	0.16598	1.1	0.6	24.91	5.51
2	0.07845	0.00021	0.00293	0.00009	24.52607	0.06279	5.5	1.2	44.21	2.11
3	0.05108	0.00054	0.00009	0.00027	16.86762	0.16090	10.5	0.4	58.19	5.27
4	0.02942	0.00010	0.00290	0.00006	10.08479	0.02993	13.8	1.9	45.70	1.08
5	0.02565	0.00008	0.00309	0.00004	8.63742	0.02349	12.3	3.7	34.78	0.85
6	0.01208	0.00005	0.00284	0.00002	4.82154	0.01584	26.0	5.5	41.14	0.66
7	0.00241	0.00004	0.00211	0.00004	1.67113	0.01175	57.3	3.2	31.43	0.50
8	0.00366	0.00002	0.00209	0.00002	2.01945	0.00711	46.4	7.3	30.76	0.39
9	0.00109	0.00004	0.00175	0.00003	1.25235	0.01105	74.2	3.5	30.48	0.47
10	0.00290	0.00001	0.00181	0.00001	1.78828	0.00438	52.0	16.4	30.51	0.34
11	0.00083	0.00001	0.00190	0.00002	1.16086	0.00438	78.8	7.8	30.01	0.33
12	0.00132	0.00002	0.00117	0.00001	1.31688	0.00484	70.4	12.3	30.40	0.34
13	0.00108	0.00002	0.00127	0.00002	1.22584	0.00504	74.0	8.3	29.78	0.34
14	0.00108	0.00001	0.00131	0.00002	1.23526	0.00364	74.1	9.3	30.02	0.32
15	0.00101	0.00003	0.00137	0.00004	1.20775	0.00923	75.2	3.5	29.79	0.42
16	0.00123	0.00002	0.00145	0.00002	1.28859	0.00620	71.7	5.8	30.31	0.36
17	0.00123	0.00002	0.00150	0.00003	1.30372	0.00684	72.0	5.0	30.82	0.38
18	0.00130	0.00006	0.00164	0.00006	1.28564	0.01696	70.2	2.4	29.61	0.63
19	0.00106	0.00006	0.00212	0.00007	1.23981	0.01766	74.7	1.9	30.41	0.66
Steps 8 - 19								83.6	30.25	0.22
Step	$^{36}Ar/^{39}Ar$	+/-	$^{37}Ar/^{39}Ar$	+/-	$^{40}Ar/^{39}Ar$	+/-	$\%^{40}Ar$	$\%^{39}Ar$	age [Ma]	+/-
Sample:	**MR-165**	J-Value: 0.01871 +/- 0.00019								
1	0.04661	0.00079	0.00621	0.00042	14.81295	0.23337	7.0	1.5	34.27	7.74
2	0.02595	0.00035	0.00522	0.00024	8.39892	0.10393	8.7	3.0	23.99	3.47
3	0.01871	0.00022	0.00498	0.00013	6.45608	0.06646	14.4	4.9	30.54	2.23
4	0.01695	0.00019	0.00501	0.00012	6.09993	0.05646	17.9	5.8	35.94	1.90
5	0.01635	0.00026	0.00463	0.00015	5.66911	0.07578	14.8	4.7	27.54	2.53
6	0.00157	0.00006	0.00336	0.00005	1.39523	0.01774	66.8	15.0	30.71	0.66
7	0.00139	0.00006	0.00326	0.00005	1.31861	0.01715	69.0	16.0	29.93	0.64
8	0.00131	0.00003	0.00318	0.00002	1.31997	0.00852	70.8	34.1	30.75	0.42
9	0.00091	0.00015	0.00380	0.00015	1.23215	0.04510	78.1	5.3	31.68	1.53
10	0.00080	0.00013	0.00352	0.00010	1.21981	0.03795	80.5	7.4	32.35	1.30
11	0.00017	0.00035	0.00576	0.00031	1.15912	0.10214	95.7	2.2	36.58	3.40
Steps 3 - 10								93.2	30.76	0.91

between each 4–5 unknown samples, which yield a distance of c. 5 mm between adjacent flux-monitors. The sealed quartz vials are irradiated in the MTA KFKI reactor (Debrecen, Hungary) for 16 hours. Correction factors for interfering isotopes have been calculated from 10 analyses of two Ca-glass samples and 22 analyses of two pure K-glass samples, which are: $^{36}Ar/^{37}Ar_{(Ca)}$ = 2.6025E-4, $^{39}Ar/^{37}Ar_{(Ca)}$ = 6.5014E-4, and $^{40}Ar/^{39}Ar_{(K)}$ = 1.5466E-2. Variation in the flux of neutrons were monitored with DRA1 sanidine standard for which a $^{40}Ar/^{39}Ar$ plateau age of 25.03 ± 0.05 Ma has been reported (Wijbrans et al., 1995). After irradiation, the minerals are unpacked from quartz vials and aluminium-foil packets and handpicked into 1 mm diameter holes within one-way Al-sample holders.

$^{40}Ar/^{39}Ar$ analyses are carried out at the Institute for Geology and Paleontology at the University of Salzburg using a UHV Ar-extraction line

Table 3 (continued).

Step	$^{36}Ar/^{39}Ar$[a]	+/-	$^{37}Ar/^{39}Ar$[b]	+/-	$^{40}Ar/^{39}Ar$[a]	+/-	%^{40}Ar[c]	%^{39}Ar	age [Ma]	+/-
Sample:	**MR-166**	J-Value: 0.01879 +/- 0.00019								
1	0.09209	0.00055	0.00115	0.00021	27.70747	0.16312	1.8	0.6	16.21	5.48
2	0.00526	0.00008	0.00210	0.00005	2.70699	0.02450	42.6	2.9	38.16	0.90
3	0.00702	0.00020	0.00426	0.00015	3.05793	0.05883	32.1	0.9	32.50	1.98
4	0.00337	0.00006	0.00379	0.00004	1.90604	0.01632	47.8	4.2	30.13	0.62
5	0.00367	0.00018	0.00398	0.00018	1.83022	0.05437	40.8	0.8	24.63	1.83
6	0.00124	0.00004	0.00289	0.00004	1.29698	0.01160	71.9	4.4	30.81	0.49
7	0.00129	0.00002	0.00275	0.00002	1.30659	0.00700	70.9	9.5	30.61	0.38
8	0.00112	0.00001	0.00265	0.00001	1.26840	0.00286	73.9	26.4	30.99	0.32
9	0.00056	0.00001	0.00249	0.00001	1.10859	0.00283	85.2	21.2	31.22	0.32
10	0.00054	0.00002	0.00235	0.00002	1.07945	0.00541	85.2	9.6	30.38	0.35
11	0.00019	0.00002	0.00129	0.00002	0.97044	0.00455	94.3	8.8	30.24	0.34
12	0.00011	0.00003	0.00123	0.00003	0.95724	0.00906	96.5	4.0	30.53	0.43
13	0.00008	0.00003	0.00110	0.00003	0.92654	0.00988	97.5	4.1	29.85	0.44
14	0.00039	0.00013	0.00304	0.00015	1.10057	0.03991	89.4	0.9	32.55	1.37
15	0.00046	0.00010	0.00134	0.00011	0.92614	0.02997	85.4	1.5	26.11	1.03
Steps 6 - 14								88.9	30.64	0.36
Step	$^{36}Ar/^{39}Ar$	+/-	$^{37}Ar/^{39}Ar$	+/-	$^{40}Ar/^{39}Ar$	+/-	%^{40}Ar	%^{39}Ar	age [Ma]	+/-
Sample:	**MR-167 I**	J-Value: 0.01894 +/- 0.00019								
1	1.34449	0.00210	0.01737	0.00033	409.99049	0.80836	3.1	0.4	388.29	22.54
2	0.15847	0.00017	0.01604	0.00007	48.82764	0.05331	4.1	3.3	66.64	1.87
3	0.01054	0.00003	0.02113	0.00002	4.33985	0.00794	28.2	22.8	40.94	0.48
4	0.00701	0.00003	0.01003	0.00003	3.08554	0.00776	32.9	12.7	33.85	0.42
5	0.00403	0.00003	0.00795	0.00003	2.22839	0.00860	46.5	9.0	34.60	0.45
6	0.00370	0.00003	0.00689	0.00003	2.09426	0.00913	47.9	8.7	33.42	0.45
7	0.00331	0.00003	0.00416	0.00002	1.89543	0.00834	48.5	10.9	30.61	0.41
8	0.00131	0.00005	0.00436	0.00006	1.26917	0.01593	69.4	2.9	29.34	0.61
9	0.00223	0.00003	0.00418	0.00003	1.53585	0.00931	57.1	7.5	29.19	0.43
10	0.00217	0.00002	0.00456	0.00002	1.55307	0.00729	58.8	8.9	30.41	0.39
11	0.00162	0.00003	0.00628	0.00003	1.44701	0.00884	67.0	7.1	32.33	0.44
12	0.00154	0.00007	0.00993	0.00007	1.35349	0.02173	66.4	2.4	29.97	0.79
13	0.00187	0.00006	0.00970	0.00006	1.50386	0.01795	63.3	3.3	31.76	0.68
Step	$^{36}Ar/^{39}Ar$	+/-	$^{37}Ar/^{39}Ar$	+/-	$^{40}Ar/^{39}Ar$	+/-	%^{40}Ar	%^{39}Ar	age [Ma]	+/-
Sample:	**MR-55**	J-Value: 0.02187 +/- 0.00022								
1	0.02466	0.00017	0.04158	0.00017	8.02935	0.05007	9.2	1.7	28.56	1.96
2	0.00777	0.00007	0.01179	0.00007	3.05275	0.02105	24.8	3.3	29.02	0.87
3	0.00539	0.00009	0.00514	0.00007	2.42513	0.02654	34.3	3.4	31.94	1.08
4	0.00178	0.00005	0.00290	0.00004	1.37186	0.01414	61.7	5.2	32.51	0.64
5	0.00115	0.00002	0.00177	0.00002	1.15008	0.00620	70.3	11.8	31.04	0.39
6	0.00039	0.00005	0.00144	0.00005	0.94929	0.01431	88.0	4.4	32.06	0.64
7	0.00056	0.00003	0.00131	0.00002	0.99248	0.00755	83.2	9.6	31.69	0.43
8	0.00059	0.00002	0.00152	0.00002	0.97717	0.00682	82.1	11.5	30.77	0.40
9	0.00045	0.00002	0.00094	0.00002	0.94806	0.00713	85.8	11.4	31.22	0.42
10	0.00040	0.00002	0.00106	0.00001	0.91675	0.00491	87.2	15.1	30.66	0.36
11	0.00044	0.00004	0.00130	0.00004	0.93373	0.01229	86.2	5.6	30.89	0.57
12	0.00032	0.00004	0.00237	0.00004	0.89497	0.01048	89.5	4.4	30.75	0.51
13	0.00033	0.00004	0.00322	0.00004	0.92596	0.01060	89.5	5.3	31.81	0.52
14	0.00030	0.00003	0.00232	0.00003	0.96905	0.00833	90.8	7.3	33.79	0.46
Steps 3 - 13								87.7	31.21	0.38

equipped with a combined MERCHANTEK™ UV/IR laser ablation facility, and a VG-ISOTECH™ NG3600 Mass Spectrometer.

Stepwise heating analyses of samples are performed using a defocused (~1.5 mm diameter) 25 W CO_2-IR laser operating in Tem_{00} mode at wavelengths between 10.57 and 10.63 µm. The laser is controlled from a PC, and the position of the laser on the sample is monitored through a double-vacuum window on the sample chamber via a video camera in the optical axis of the laser beam on the computer screen. Gas clean-up is performed using one hot and one cold Zr-Al SAES getter. Gas admittance and pumping of the mass spectrometer and the Ar-extraction line are computer controlled using pneumatic valves. The NG3600 is a 18 cm radius 60° extended geometry instrument, equipped with a bright NIA-type source operated at 4.5 kV. Measurement is performed on an axial electron multiplier in static mode, peak-jumping and stability of the magnet is controlled by a Hall-probe. For each increment the intensities of ^{36}Ar, ^{37}Ar, ^{38}Ar, ^{39}Ar and ^{40}Ar are measured, the baseline readings on mass 35.5 are automatically subtracted. Intensities of the peaks are back-extrapolated over 16 measured intensities to the time of gas admittance either by a straight line or a curved fit. Intensities are corrected for system blanks, background, post-irradiation decay of ^{37}Ar, and interfering isotopes. Isotopic ratios, ages and errors for individual steps are calculated following suggestions by McDougall and Harrison (1999) using decay factors reported by Steiger and Jäger (1977). Definition and calculation of plateau ages has been carried out using ISOPLOT/EX (Ludwig, 2001).

Results

Results from Ar stepwise heating analyses are presented in Table 3 and graphically portrayed as age-spectra in Fig. 5. The plateau ages are inverse variance-weighted averages of single steps meeting the criteria for plateau-ages after Ludwig (2001) with errors at 95% confidence level; the J-value can be estimated only roughly and due to its propagation into the error of the single heating steps, the uncertainties of the errors of the J-values may influence the errors of the plateau ages to some extend. Table 4 summarises the interpretation of the obtained ages and Fig. 6 depicts the results in relation to other geologic events. Except for Ar analysis of white mica from MR 167 I, analyses from all samples yielded more or less concordant age spectra, with minor fluctuations in the first low-temperature gas release steps only. As the grain size of all samples exceeds ~60 µm (Table 1), the effects of ^{39}Ar recoil loss are less than 0.5% and can be neglected (Foland et al., 1992).

Laki ore field

Age spectra from the Laki ore field (white mica samples MR 20 and MR 20A) display well-developed, almost undisturbed plateaus corresponding

Table 3 (continued).

Step	$^{36}Ar/^{39}Ar^a$	+/-	$^{37}Ar/^{39}Ar^b$	+/-	$^{40}Ar/^{39}Ar^a$	+/-	$\%^{40}Ar^c$	$\%^{39}Ar$	age [Ma]	+/-
Sample:	**MR-46 Ia**	J-Value: 0.02194 +/- 0.00022								
1	0.01742	0.00034	0.00871	0.00024	5.97445	0.10086	13.8	0.9	31.83	3.94
2	0.00920	0.00006	0.00303	0.00004	3.39999	0.01726	20.0	5.5	26.17	0.72
3	0.00667	0.00006	0.00231	0.00005	2.69224	0.01681	26.8	5.3	27.76	0.71
4	0.00270	0.00003	0.00112	0.00003	1.63891	0.01021	51.3	9.9	32.39	0.51
5	0.00519	0.00004	0.00125	0.00003	2.45289	0.01261	37.5	9.6	35.44	0.60
6	0.00331	0.00003	0.00108	0.00002	1.87704	0.00892	47.8	11.5	34.60	0.49
7	0.00453	0.00006	0.00100	0.00004	2.24358	0.01697	40.4	5.8	34.91	0.74
8	0.00334	0.00003	0.00051	0.00003	1.91231	0.01005	48.4	9.5	35.68	0.53
9	0.00381	0.00004	0.00087	0.00003	2.05726	0.01091	45.3	10.0	35.90	0.55
10	0.00306	0.00003	0.00079	0.00002	1.82761	0.00855	50.6	10.9	35.63	0.49
11	0.00020	0.00008	0.00098	0.00009	0.98274	0.02353	93.9	2.6	35.55	0.98
12	0.00015	0.00006	0.00039	0.00010	0.94619	0.01905	95.4	3.1	34.80	0.82
13	0.00017	0.00005	0.00097	0.00006	0.97493	0.01473	94.8	4.7	35.60	0.67
14	0.00007	0.00002	0.00008	0.00003	0.92075	0.00728	97.8	8.3	34.70	0.45
15	0.00021	0.00008	0.00028	0.00011	0.96539	0.02371	93.6	2.3	34.82	0.98
Steps 5 - 15								78.4	35.25	0.36

For all samples:
*Ages are inverse variance-weighted averages of single steps meeting the criteria for plateau-ages after Ludwig (2001) with errors at 95% confidence level; errors of ratios, J-values and single steps are at 1s level
a) measured
b) corrected for post-irradiation decay of ^{37}Ar (35.1 days)
c) non atmospheric ^{40}Ar

Table 4 $^{40}Ar/^{39}Ar$ plateau ages of white micas from the Central Rhodopian Dome.

	Sample Nr.	Age (Ma)	Interpretation
Laki ore field	MR CH	29.36 – 0.34	Ore formation age
	MR 20	35.28 – 0.22	Metamorphic cooling or pre-ore alteration age
	MR 20A	36.13 – 0.31	Metamorphic cooling or pre-ore alteration age
	MR 23	29.37 – 0.29	Ore formation age
	MR 170	29.19 – 0.44	Ore formation age
Madan ore field	MR 71B	31.55 – 0.46	Age of ore-related alteration
	MR 158 Ia	29.95 – 0.23	Ore formation age
	MR 164	30.25 – 0.22	Ore formation age
	MR 165	30.76 – 0.91	Ore formation age
	MR 166	30.64 – 0.36	Ore formation age
	MR 167 I	no plateau	Alteration / excess Argon
Eniovche dep.	MR 55	31.21 – 0.38	Age of alteration halo
	MR 62 Ia	25.00 – 0.54	Resetting of the system
Davidkovo ore field	MR 46 Ia	35.25 – 0.36	Cooling age

to ages of 35.28 ± 0.22 Ma (steps 4–15, 92.8% ^{39}Ar released) and 36.13 ± 0.31 Ma (steps 5–11, 91% ^{39}Ar released) respectively. Slightly younger ages recorded in the first low-temperature gas release steps (~30 Ma) may indicate minor isotopic loss of radiogenic ^{40}Ar subsequent to initial isotopic closure. White mica from sample MR 20 fills a small cavity in altered gneiss in the vicinity of a Mn-skarn alteration front. The age of ~35 Ma therefore is interpreted to be related to regional metamorphism, but could also date alteration related to early skarn formation. The sample MR20A is located at the front of the metasomatic replacement body to the marble horizon and shows a weak foliation overgrown by crosscutting epidote needles. Since the radially arranged epidote crystals are not affected by any deformation, this sample obtained its muscovite alignment before or during one of the pre-ore tectonic phases and before the metasomatic replacement by Mn-skarns, but it could also have been reset from an even older metamorphic age during metasomatic Mn-skarn formation. Muscovite crusts and crystals linked to Pb–Zn sulphide precipitation MR 23, MR CH, and MR 170 again display concordant age spectra, which are significantly younger compared to samples MR 20 and MR 20A. Sample MR 23 reveals an almost flat Ar-release plot, recording a well-defined plateau age of 29.37 ± 0.29 Ma (steps 5–14; 91.0% ^{39}Ar released). The white mica crust on a quartz crystal in sample MR CH revealed a slightly disturbed age pattern indicating minor ^{40}Ar-loss in the first 4 increments of the experiment. However, a plateau (steps 5–11; 70.9% ^{39}Ar released) yielding an age of 29.36 ± 0.34 Ma is calculated which is identical to the result of MR23. Analysis of white mica from sample MR 170 again displays a flat Ar-release pattern, recording a plateau age of 29.19 ± 0.44 Ma for steps 3–9 (91.0% ^{39}Ar released).

Madan ore field and Eniovche deposit

White mica derived from hydrothermal alteration of the gneisses MR 55 and MR 71 B yields plateau ages of 31.21 ± 0.38 Ma (steps 3–13; 87.7% ^{39}Ar released) and 31.55 ± 0.46 Ma (steps 6–17; 75.3% ^{39}Ar released) respectively, although the Ar-release spectrum of sample MR 71B indicates isotopic disturbances in the first 5 (24.7% ^{39}Ar released) increments. These disturbances are interpreted to be the result of outgassing of another, less retentive and more Ca-rich mineral phase (see Table 3 for $^{37}Ar/^{39}Ar$ ratios), or chemical alteration of the micas that was not detected during mineral purification. Muscovites occurring as crusts and globular crystals between stages of Pb–Zn sulphide precipitation and overgrowing euhe-

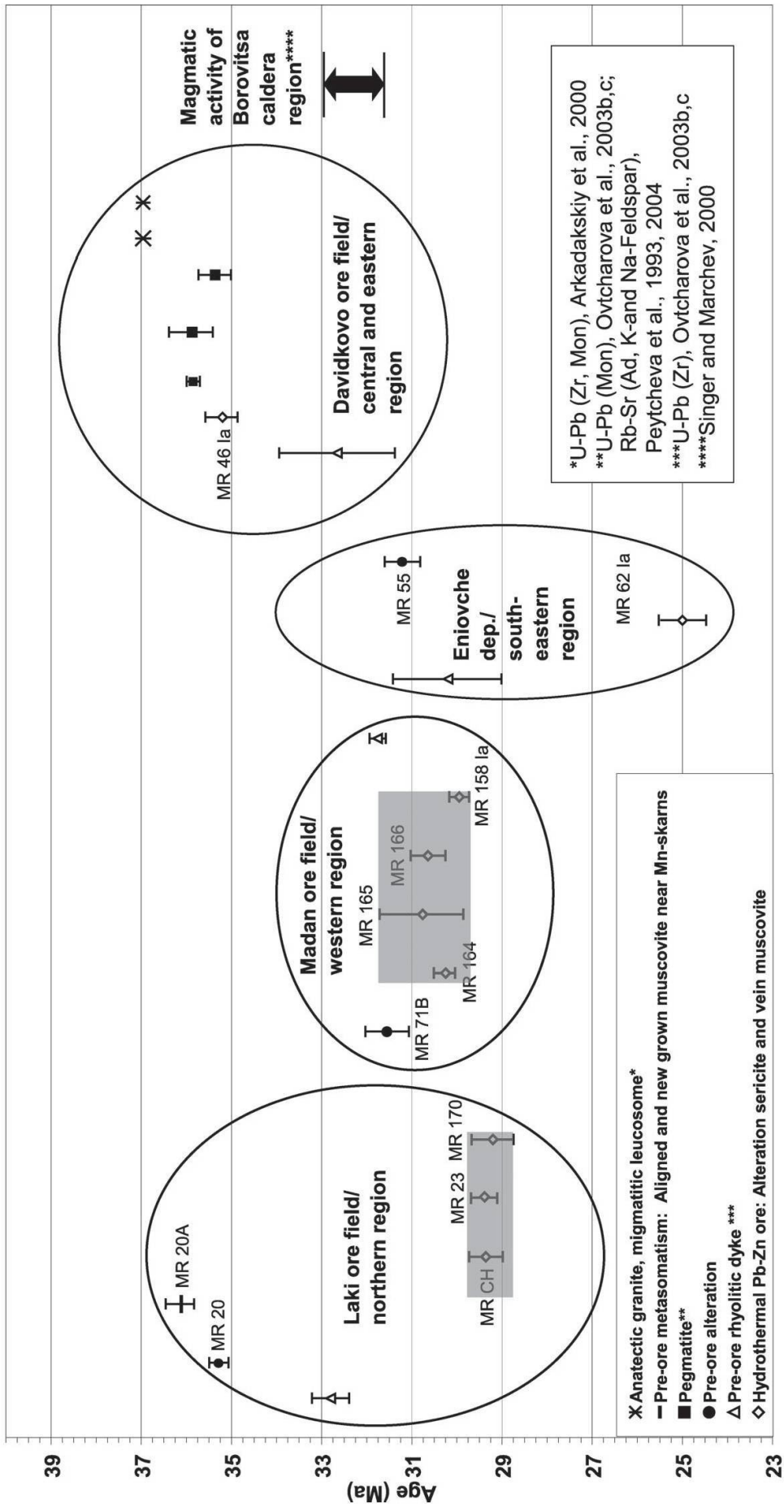

Fig. 6 Summary of currently available high-precision age data, including Ar–Ar data from hydrothermal muscovite (this study) and published information from Ovtcharova et al. (2003b,c), Peytcheva et al. (1993, 2004), Singer and Marchev (2000).

dral vug crystals from samples MR 158 Ia, MR 164, MR 165, and MR 166 display flat Ar-release spectra with plateau ages of 29.95 ± 0.23 Ma, 30.25 ± 0.22 Ma, 30.76 ± 0.91 Ma, and 30.64 ± 0.36 Ma, respectively. Analysis of texturally similar white mica from orebody MR 62 Ia displays a disturbed age pattern: The first 5 steps (together comprising 29.0% of the ^{39}Ar released) yielded ages ranging from 23 to 31 Ma; a plateau age of 25.00 ± 0.54 Ma can be calculated for steps 6–16 (71.0% ^{39}Ar released) probably reflecting hydrothermal processes accompanying and succeeding ore deposition which might have caused resetting of the system. Therefore, the question about persisting hydrothermal activity must be raised which could be the subject of ongoing studies. Globular muscovite crystals connected to galena and sphalerite precipitation MR 167 I display a completely disturbed Ar-release pattern with likely excess Argon leading to meaningless ages ranging between 67 and 29 Ma. Microscopic studies show dissolved surfaces of galena indicating that postdepositional leaching has affected this sample.

Davidkovo ore field

A single sample MR 46 Ia of untypically coarse-grained muscovite that texturally predates galena and sphalerite precipitation in vugs reveals a "disturbed" age pattern, with ages increasing from ~26 to ~35 Ma in the low-temperature gas-release steps (together comprising 21.6% ^{39}Ar released). Intermediate to high-temperature gas release steps define a plateau age of 35.25 ± 0.36 Ma (steps 5–15; 78.4% ^{39}Ar released), which is significantly older than the mineralisation ages from the other ore fields and may be related to a late-metamorphic pre-ore fluid event.

Late-orogenic extension, uplift and hydrothermal ore formation in the Central Rhodopian Dome

Figure 6 summarizes the relationship between our new Ar–Ar data on hydrothermal muscovites and published ages of magmatism and regional metamorphism (Arkadakskiy et al., 2000; Singer and Marchev, 2000; Peytcheva et al., 1993, 2004; Ovtcharova et al., 2003b, 2003c). The earliest event in the Central Rhodopian Dome recorded by our new Ar–Ar data is the apparently undisturbed metamorphic age spectrum of muscovite flakes in the contact of the Mn-skarn of Laki (sample MR 20A). This age is very close to that from an altered gneiss near the Mn-skarn front (MR20) and to the above mentioned ages of a migmatic leucosome in the center of the dome of about 37 Ma (Arkadaksky et al., 2000; Ovtcharova et al., 2003a), a chamber pegmatite near Latinka in the southeastern part of the dome (35.31 ± 0.25 Ma; Rb–Sr on feldspar-adularia; Peytcheva et al., 2004) and a massive pegmatite near Chepelare in northwestern direction (35.89 ± 0.15 Ma; concordant U–Pb age on monazite single grains; Ovtcharova et al., 2003b, 2003c). This temporal relation at ~36–37 Ma could indicate a genetic relation between pegmatites and the earliest stages of metasomatic replacement, which might have been driven by residual hydrothermal fluids originating from the crystallisation of deep-seated felsic magmas of likely crustal-anatectic origin followed by uplift and cooling of the footwall of the dome. The coarse grained hydrothermal muscovite MR 46 Ia from Davidkovo also records an age around 35 Ma. Two plateau ages of white mica derived from hydrothermal alteration MR 71b and MR55 are interpreted to date pre- to syn-ore alteration of quartz–sericite–pyrite–epidote type around 31 Ma. White mica crusts and globular crystals grown in open vugs have been deposited contemporarily with the main ore stage clustering around 30.4 Ma at Madan and about 1 Ma later around 29.3 Ma in the Laki ore field (grey boxes in Fig. 6).

The currently available results clearly show that, within a period of 5 Ma or less, the area of the Central Rhodopian Dome was subject to large-scale extensional detachment, uplift of the footwall unit of the dome to within <2 km from the present surface, and cooling of the center of the dome from upper amphibolite facies conditions to less than 250 °C. The exact time relation between rhyolitic magmatism and hydrothermal ore formation remains to be fully investigated. The time span of magmatism in Borovitsa area is estimated by Ar–Ar-dating on magmatic silicates as 33–31.75 Ma (Ar–Ar on biotite, K-feldspar, plagioclase and alunite; Singer and Marchev, 2000). Similar ages would be consistent with crosscutting relations between gneisses, detachment, rhyolitic dykes and Pb–Zn veins at Madan and Laki, as confirmed by preliminary U–Pb data for some of these dykes by Ovtcharova et al. (2003b, 2003c; Fig. 6). We cannot decide at this stage whether upper-crustal silicic magmatism contributed directly to hydrothermal fluid flow (e.g. from magma chambers at slightly deeper upper-crustal levels), or whether even larger-scale hydrothermal fluid flow was driven by the high heat flow attending rapid uplift of the dome from high-grade metamorphic conditions into the near-surface regime allowing brittle fracturing. The close proximity in time of acid magmatism and hydrothermal

ore formation indicates that both processes are ultimately driven by the large-scale thermal disturbance of metamorphic core complex formation and rapid uplift attending tectonic and erosional denudation in the final stages of orogenic collapse.

Acknowledgements

This investigation is supported by the Institute of Isotope Geochemistry and Mineral Resources at ETH Zurich and the Institute for Geology and Palaeontology at Salzburg University. Special thanks go to colleagues in the Fluids and Mineral Deposits Group at ETH Zürich, notably to Thomas Driesner for his support during field trips and sample assessment and to Thomas Pettke, Claudia Pudack and Irena Peytcheva for critical discussions. Special thanks go to Felix Oberli for help with data evaluation as well as to the reviewers Niko Froitzheim, Peter Marchev and Chris Hall for further valuable inputs. We also want to thank our Bulgarian colleagues Ivan Bonev, Zlatka Cernova, Zhivko Ivanov, Paraskev Petrov and Petko Petrunov for logistic support and scientific guidance during field work. Irene Ivanov and Walter Wittwer provided essential help with mineral separation. This project is funded by the Swiss National Science Foundation (No. 2000-59544.99 and 200020-100735/1) and by the European Science Foundation through the GEODE (Geodynamics and Ore Formation) Programme.

References

Amov, B., Baldjieva, T., Breskovska, V., Dimitrov, R.B.K., Stoikov, C. and Todorov, T. (1985): Isotopic composition of lead, origin and age of deposits in south Bulgaria. *Geologija Rudnyich Mjestororozhdenij* **3**, 3–17 (in Russian).

Amov, B., Kolkovski, B. and Dimitrov, R. (1993): Genesis and age of hydrothermal ore mineralization in the Rhodope metallogenic zone on the basis of the isotopic composition of lead in galena. *Annuaire de l'Université de Sofia "St. Kliment Ohridski" Faculté de Géologie et Géographie* **85**, 73–98 (in Bulgarian).

Arkadakskiy, S., Böhm, S.C., Heaman, L., Cherneva, Z. and Stancheva, E. (2000): New U–Pb results from the central Rhodope Mts., Bulgaria. In: Bogdanov, K. (ed.): Geodynamics and Ore Deposit Evolution of the Alpine-Balkan-Carpathian-Dinaride-Province. Borovets, p. 5.

Beaudoin, G., Taylor, B.E. and Sangster, D.F. (1991): Silver-lead-zinc veins, metamorphic core complexes, and hydrologic regimes during crustal extension. *Geology* **19**, 1217–1220.

Beaudoin, G., Taylor, B.E. and Sangster, D.F. (1992): Silver-lead-zinc veins and crustal hydrology during Eocene extension, southeastern British-Columbia, Canada. *Geochim. Cosmochim. Acta* **56**, 3513–3529.

Blundell, D.J., Neubauer, F. and v. Quadt, A. (2002): The timing and location of major ore deposits in an evolving orogen. Geol. Soc. London Spec. Publ. **204**, 353 pp.

Bonchev, G. (1915): Kristalinnite skali v Bulgaria. *Godishnikh na Sofiyskiya Universitet Geologo-Geografski Fakultet* **10–11/2**, 1–127.

Bonev, I. (1968): Pseudomorphose der Pyroxene aus den Skarnlagern im Madaner Erzrevier. *Geochem. Mineral. and Petrol.* **27**, 221–240 (auf Bulgarisch).

Bonev, I. (1982): Madan – lead-zinc vein and metasomatic ore deposits; Guide-Book 3: Central Rhodopes. In: Acad. Sci. Soc. 13th General Meeting. Varna, Bulgaria.

Bonev, I. (1984): Mechanisms of the hydrothermal ore deposition in the Madan lead-zinc deposits, central Rhodopes, Bulgaria. In: Janelidze, T. and Tvalchrelidze, A. (eds.): Proceedings of the Sixth quadrennial IAGOD symposium. Stuttgart, International, 69–73.

Bonev, I., Boyce, A.J., Fallick, A.E. and Rice, C.M. (2000): Ore fluids, stable isotopes and ore-forming processes in the Tertiary Pb–Zn vein and replacement ore deposits of the Madan district. In: Bogdanov, K. (ed.): Geodynamics and Ore Deposit Evolution of the Alpine-Balkan-Carpathian-Dinaride-Province. Borovets, p. 13.

Bonev, I.K. (1977): Primary fluid inclusions in galena crystals. 1. Morphology and origin. *Mineralium Deposita* **12/1**, 64–76.

Burg, J.P., Ivanov, Z., Ricou, L.E., Dimor, D. and Klain, L. (1990): Implications of shear-sense criteria for the tectonic evolution of the central Rhodope Massif, southern Bulgaria. *Geology* **18/5**, 451–454.

de Boorder, H., Spakman, W., White, S.H. and Wortel, M.J.R. (1998): Late Cenozoic mineralization, orogenic collapse and slab detachment in the European Alpine Belt. *Earth Planet. Sci. Lett.* **164**, 569–575.

Dimitrov, S. (1946): Metamorfnite i magmatichnite skali v Bulgaria. *God. Dir. geol. u minni prouchv.* **A/4**, 61–93.

Dimov, D., Dobrev, S., Ivanov, Z., Kolkovski, B. and Sarov, S. (2000). In: Ivanov, Z. (ed.): Structure, alpine evolution and mineralizations of the central Rhodopes area (south Bulgaria). Geodynamics and ore deposits evolution of the Alpine-Balkan-Carpathian-Dinaride province Guide to Excursion B. University Press "St. Kliment Ohridski", Borovets, Bulgaria, 50 pp.

Dragiev, H. and Danchev, J. (1990): Morphological-structural specialities of metasomatic deposits in the Erma Reka area in the Madan's ore field. Geologica Rhodopica 2. Aristotle University Press, Thessaloniki.

Foland, K.A., Hubacher, F.A. and Arehart, G.B. (1992): $^{40}Ar/^{39}Ar$ dating of very fine-grained samples: An encapsulated-vial procedure to overcome the problem of ^{39}Ar recoil loss. *Chemical Geology* (Isotope Geoscience section) **102**, 269–276.

Georgieva, M., Cherneva, C., Kolcheva, K., Sarov, S., Gerdjikov, J. and Voinova, E. (2002): Scientific meeting of the Geological Institute BAS, Sofia University.

Heinrich, C.A. and Neubauer, F. (2002): Cu-Au-Pb-Zn-Ag metallogeny of the Alpine-Balkan-Carpathian-Dinaride geodynamic province. *Mineralium Deposita* **37/6–7**, 533–540.

Ivanov, Z. (1988): Aperçu général sur l'évolution géologique et structurale du massif des Rhodopes dans le cadre des Balkanides. *Bull. Soc. géol. France* **8/4**, 227–240.

Ivanov, Z. (1989): Structure and tectonic evolution of the central parts of the Rhodope massif. Guide to excursion E3, CBGA-XIV congress. 126 pp.

Jankovic, S. (1977): The copper deposits and geotectonic setting of the Tethyan Eurasian metallogenic belt. *Mineralium Deposita* **12**, 37–47.

Jankovic, S. (1997): The Carpatho-Balkanides and adjacent area: A sector of the Tethyan Eurasian metallogenic belt. *Mineralium Deposita* **32/5**, 426–433.

Kober, L. (1928): Die Grossgliederung der Dinariden. Borntraeger, Berlin, 499 pp.

Kolkovski, B., Dobrev, S., Petrov, P. and Manev, D. (1996): Geology, mineralogy and genesis of Madan ore field. In: Popov, P. (ed.): Plate Tectonic Aspects of the Alpine Metallogeny in the Carpatho-Balkan-Region. Sofia, 157–173.

Kolkovski, B., Melnikov, F.P. and Petrov, P. (1978): Temperature of mineral forming in base metal deposits from Madan ore field (Bulgaria). Theory and practice of thermobarogeochemistry. *M. Nauka*, 116–118 (in Russian).

Kolkovski, B. and Petrov, P. (1972): On temperature of ore forming in deposits along Spoluka-Laikov choukar fault, Madan district. *Annuaire de l'Université de Sofia "St. Kliment Ohridski" Faculté de Géologie et Géographie* **64/1**, 225–233.

Kostova, B. and Petrov, P. (2003): Fluid inclusion study on the Yuzhna Petrovitsa Pb–Zn deposit, Madan ore field, central Rhodopes, Bulgaria. In: Neubauer, F. and Handler, R. (eds.): Geodynamics and Ore Deposit Evolution of the Alpine-Balkan-Carpathian-Dinaride Province. Seggauberg, Austria, 33–34.

Kostova, B., Pettke, T., Driesner, T., Petrov, P. and Heinrich, C.A. (2004): LA ICP-MS study of fluid inclusions in quartz from the Yuzhna Petrovitsa deposit, Madan ore field, Bulgaria. *Schweiz. Mineral. Petrogr. Mitt.* **84**, 25–36.

Krasteva, M. and Stoynova, M. (1988): Fluid inclusions in quartz from the deposits in the Laki ore field, Central Rhodope Mts. *Geochem. Mineral. and Petrol.* **24**, 41–54 (in Bulgarian).

Lilov, P., Yanev, Y. and Marchev, P. (1987): K/Ar dating of the eastern Rhodope Paleogene magmatism. *Geologica Balcanica* **17/6**, 49–58.

Lips, A.L.W., White, S.H. and Wijbrans, J.R. (2000): Middle–Late Alpine thermotectonic evolution of the Rhodope Massif, Greece. *Geodinamica Acta* **13**, 1–12.

Lips, A.L.W. (2002): Cross-correlating geodynamic processes and magmatic-hydrothermal ore deposit formation over time; a review in Southeast Europe. In: Blundell, D.J., Neubauer, F. and v. Quadt, A. (eds.): The timing and location of major ore deposits in an evolving orogen. *Geol. Soc. London Spec. Publ.* **204**, 69–79.

Ludwig, K.R. (2001): ISOPLOT/EX: 2.49 ed. Berkeley Geochronol. Cent. Spec. Pub. 1a.

Maneva, B., Naphtali, L., Manev, D. and Kolkovski, B. (1996): Central Rhodope Late Alpine Base Metal Ore District – General Overview and Metallogeny. In: Popov, P. (ed.): Plate Tectonic Aspects of the Alpine Metallogeny in the Carpatho-Balkan-Region. Sofia, 107–116.

McDougall, I. and Harrison, M. T. (1999): Geochronology and thermochronology by the $^{40}Ar/^{39}Ar$ Method. 2. ed. Oxford University Press, New York, Oxford.

Meyer, W. (1968): Altersstellung des Plutonismus im Südteil der Rila-Rhodope-Masse. *Geol. Paläont.* **2**, 173–192.

Meyer, W. (1969): Die Faltenachsen im Rhodopenkristallin östlich des Strimon (Nordost-Griechenland). *Geotekt. Forsch.* **31**, 86–96.

Milev, V., Stanev, V. and Ivanov, V. (1996): Mining production in Bulgaria. 1878–1995, statistical reference book. Zemia-93 Press, 196 pp.

Mitchell, A.H.G. (1996): Distribution and genesis of some epizonal Zn–Pb and Au provinces in the Carpathian-Balkan region. *Transactions of the institution of mining and metallurgy section B-applied earth science* **105**, B127-B138.

Mposkos, E. and Krohe, A. (2000): Petrological and structural evolution of continental high pressure (HP) metamorphic rocks in the Alpine Rhodope Domain (N. Greece). In: Panayides, J., Xenophontos, C. and Malpas, J. (eds.): Proceedings of the third international conference on the Geology of the eastern Mediterranean. Ministry of Agriculture, Natural Resources and Environment, Geological Survey Department. Nicosia, Cyprus.

Naphtali, L. and Malinov, O. (1988): Davidkovo ore field. In: Lead-zinc deposits in Bulgaria. *Technika*, 64–71.

Ovtcharova, M., v. Quadt, A., Peytcheva, I., Neubauer, F., Heinrich, C.A. and Kaiser, M. (2003a): Time and duration of metamorphism and exhumation of the central Rhodopian core complex, Bulgaria. Geophysical Research Abstracts 5/10121.

Ovtcharova, M., von Quadt, A., Cherneva, Z., Peycheva, I., Heinrich, C.A., Kaiser-Rohrmeier, M., Neubauer, F. and Frank, M. (2003b): Isotope and geochronological study on magmatism and migmatitization in the Central Rhodopian core complex, Bulgaria. In: Neubauer, F. and Handler, R. (eds.): Geodynamics and ore deposit evolution of the Alpine-Balkan-Carpathian-Dinaride province. Seggauberg, Austria. p. 42.

Ovtcharova, M., von Quadt, A., Heinrich, C.A., Frank, M., Kaiser-Rohrmeier, M., Peycheva, I. and Cherneva, Z. (2003c). Triggering of hydrothermal ore mineralization in the Central Rhodopean Core Complex (Bulgaria) – Insight from isotope and geochronological studies on Tertiary magmatism and migmatization. In: Demetrios et al. (eds.): Mineral exploration and sustainable development. Millpress, Rotterdam, 151–178.

Pereira, J. and Dixon, C.J. (1971): Mineralisation and Plate Tectonics. *Mineralium Deposita* **6**, 404–405.

Peytcheva, I., von Quadt, A., Ovtcharova, M., Handler, R., Neubauer, F., Salnikova, E., Kostitsyn, Y., Sarov, S. and Kolcheva, K. (2004): Metagranitoids from the eastern part of the Central Rhodopean Dome (Bulgaria): U–Pb, Rb–Sr and $^{40}Ar/^{39}Ar$ timing of emplacement and exhumation and isotope-geochemical features. *Mineralogy and Petrology* **82**, 1–31.

Peytcheva, I., Kostiyin, Y., Salnikova, Y., Kamenov, B. and Klayn, L. (1998): Rb–Sr and U–Pb isotope data for the Rila-Rhodopes batholith. *Geochem. Mineral. Petrol.* **35**, 93–105 (in Bulgarian, abstract in English).

Peytcheva, I., Sokolov, S. and Sekiranov, A. (1993): Rb–Sr isotopic data obtained on pegmatites from the town of Ardino region, Central Rhodopes. *Comptes rendus de l' Académie bulgare des Sciences* **46/7**, 63–65 (in Bulgarian).

Piperov, N.B., Penchev, N.B. and Bonev, I.K. (1977): Primary fluid inclusions in galena crystals. 2. Chemical Composition of the liquid and gas phase. *Mineralium Deposita* **12**, 77–89.

Ricou, L.-E., Burg, J.-P., Godfriaux, I. and Ivanov, Z. (1998): Rhodope and Vardar: the metamorphic and the olistostromic paired belts related to the Cretaceous subduction under Europe. *Geodinamica Acta* **11/6**, 1–25.

Sawkins, F.J. (1984): Metal deposits in relation to plate tectonics. *Minerals, rocks and inorganic materials* **17**. Berlin, 325 pp.

Sillitoe, R.H. (1991): Gold metallogeny of Chile – an introduction. *Economic Geology* **86**, 1187–1205.

Singer, B. and Marchev, P. (2000): Temporal evolution of arc magmatism and hydrothermal activity including epithermal gold veins, Borovitsa caldera, southern Bulgaria. *Economic Geology* **95**, 1155–1164.

Spencer, J.E. and Welty, J.W. (1986): Possible controls of base- and precious-metal mineralization associated with Tertiary detachment faults in the lower Colorado River trough, Arizona and California. *Geology* **14**, 195–198.

Steiger, R.H. and Jäger, E. (1977): Subcommission on Geochronology – convention on use of decay constants in geochronology and cosmochronology. *Earth Planet. Sci. Lett.* **36/3**, 359–362.

Tzvetanov, R. (1976): Hydrothermal metasomatites in the "Charaaliev Dol – Petrovitsa" fault of the Madan ore field. *Annuaire de l'Université de Sofia "St. Kliment Ohridski" Faculté de Géologie et Géographie* **67/1**, 296–308.

Vassileva, R.D. and Bonev, I. (2001): Mineral relations and paragenetic sequences in the skarn and post-skarn in the Pb–Zn ore deposits, Central Rhodopes. *Romanian Journal of Mineral Deposits* **79/2**, 101–102.

von Blanckenburg, F. and Davies, J.H. (1995): Slab breakoff – a model for syncollisional magmatism and tectonics in the Alps. *Tectonics* **14/1**, 120–131.

Wijbrans, J.R., Pringle, M.S., Koopers, A.A.P. and Schveers, R. (1995): Argon geochronology of small samples using the Vulkaan argon laserprobe. In: Kon. Ned. Akad. v. Wetensch. **98/2**, 185–218.

Wortel, M.J.R. and Spakman, W. (2000): Geophysics – Subduction and slab detachment in the Mediterranean-Carpathian region. *Science* **290**, 5498, 1910–1917.

Received 15 December 2003
Accepted in revised form 24 June 2004
Editorial handling: T. Driesner and A. von Quadt